

Ref. Ares(2021)1532258 - 27/02/2021

ID-FAST - Investigations on degradation mechanisms and Definition of protocols for PEM Fuel cells Accelerated Stress Testing

Grant agreement no: 779565

Call: H2020-JTI-FCH-2017-1

D4.2 – Analysis of state of art AST and definition of single components AST

Authors:	Andrea Casalegno, Andrea Baricci, Andrea Bisello, Elena Colombo (POLIMI) Pawel Gazdzicki, Krishan Talukdar (DLR) Fabrice Micoud, Sylvie Escribano (CEA)
Confidentiality	PUBLIC
First issue date	20.01.2021
Submission date	26.02.2021

**Revisions**

<i>Version</i>	<i>Date</i>	<i>Authors</i>	<i>Comments</i>
1	20.01.2021	Andrea Casalegno (POLIMI)	Report structured
2	08.02.2021	Pawel Gazdzicki (DLR)	Contribution to chapter 5 added
3	22.02.2021	Fabrice Micoud, Sylvie Escribano (CEA)	Addition of protocols and results on CCL <i>operando</i> ASTs developed based on SoA ASTs.
4	24.02.2021	Andrea Casalegno, Andrea Baricci, Andrea Bisello, Elena Colombo (POLIMI)	Addition of Polimi inputs about zero gradient cell, SoA, analysis of SU/SD and new AST for start-up. Summary as report leader.
5	25.02.2021	Sylvie Escribano (CEA) Andrea Bisello (POLIMI)	Revisions and addition of last inputs
final	26.02.2021	Sylvie Escribano (CEA)	Final check as coordinator before submission



Summary

The overall aim for the period was to continue studying the impact of stressors for single mechanisms or single components as a basis for the definition of combined ASTs.

The remaining activities on testing tools and methodology have been finalized. Suitable operating conditions for performance characterization adopting zero-gradient single cell have been defined to evaluate cell components performance. The definition of conditions for polarization curves started from the analysis of ID-FAST driving cycle and considered the heterogeneities that typically occurs in a full-scale cell. Polimi designed and realized an opensource zero gradient cell, named Zero-P, that has been validated through comparison with the other zero gradient hardware available in the Consortium.

A comprehensive analysis of the major degradation mechanisms occurring in PEMFC during automotive operation and of the state of art. AST's was carried out, identifying the necessary improvement to be included in the combined AST to develop. The reference MEA has been tested in the zero-gradient hardware under the most common AST's (electrocatalyst, support and membrane) and characterized adopting the mentioned shared operating conditions to set a basis for AST development.

Two steps load cycle under actual PEMFC operation was proposed as possible AST to evaluate catalyst degradation. Dwell time during current step (12s/12s vs. 6s/6s) plays an important role of stressor and quicker performance loss was observed for higher dwell time. No significant impact of RH up to 80% was observed in two-steps load cycles, but stressing effect of water with gases humidified at more than 100% is tested. For this type of operando AST tests, specific OCV periods and start-up/shut-down event with H₂/air front, were defined and added to the two-steps load cycles and indeed showed accelerating impact. Conclusions on the stressors will be validated by testing their effect on different MEAs and then used to improve the operando combined ASTs to be applied on single cells or stacks.

Regarding AST's specific to GDL, the effect of possible stressors for GDL has been systematically investigated, the conclusion is that none of the identified AST's selectively degrade GDL significantly, in all cases CCM degradation dominates. This is likely due to the high stability of the tested GDL's in the automotive application.

The start-up and shut-down processes, identified as critical towards degradation of cathode catalyst layer, have been systematically studied mimicking real operation that includes the effect of mitigation strategies widely adopted by powertrain developers. The dynamics of such processes have been analysed in detail, permitting to obtain, supported by modelling analysis (cf. public deliverable D3.2 "Simulation report on multi-mechanisms degradation modes"), a solid interpretation of the occurring phenomena.

The mitigated conditions have been investigated performing several hundreds of start-up cycle in a segmented cell, revealing the highly heterogeneous degradation and identifying Pt dissolution as the major degradation mechanism. Being the state-of-art AST for catalyst support inappropriate to reproduce the effects of start-up under such mitigated conditions, a new Start-up AST protocol has been developed and demonstrated to be representative of degradation caused by mitigated start-up process.



Table of content

Summary	3
List of Abbreviations	5
List of symbols.....	5
1. Introduction.....	6
2. Characterization protocols for zero-gradient Fuel Cell	6
Description of Zero-P reference hardware.....	8
3. State of Art analysis of AST and identification of necessary improvements	11
Electrocatalyst AST.....	12
Carbon support AST	14
Membrane AST.....	16
4. Analysis of stressors in catalyst layer degradation.....	17
Description of the protocols.....	18
Results and discussion	21
Conclusions and next steps:	26
5. Development of GDL specific ASTs and effect of stressors	27
6. Extended analyses of start-up/shut-down	34
7. Development of a new AST related to start-up	39
Start-up/shut-down protocols	39
Degradation analysis under un-mitigated start-up/shut-down protocol	41
Degradation analysis under mitigated start-up/shut-down protocol.....	42
New Start-up AST	46
Accelerated start-up AST and further validation till 1000 cycles.	50
Analysis to improve acceleration factor	50



List of Abbreviations

AST	Accelerated Stress Test
BOL	Begin of Life
BOT	Begin of Test
CCM	Catalyst Coated Membrane
CL	Catalyst Layer
CV	Cyclic Voltammetry
ECSA	Electrochemically active Surface Area
EIS	Electrochemical Impedance Spectroscopy
EOL	End of Life
EOT	End of Test
GDL	Gas Diffusion Layer
JRC	Joint Research Center of the European Commission
MEA	Membrane Electrode Assembly
RH	Relative Humidity

List of symbols

F	Faraday constant
$\lambda_{\text{fuel/ox}}$	Fuel (anode) / oxidant (cathode) stoichiometry
T	Temperature
$p_{\text{abs/g}}$	Absolute / Gauge (<i>i.e.</i> over-) pressure
Δ	Difference



1. Introduction

To identify the transfer function from AST to real ageing mechanisms in single cell, including the effect of stressing operating condition and coupling between different degradation mechanisms, the ID-FAST project has conducted an extensive analysis of the single degradation mechanisms that affect the MEA components.

The activity started with the analysis of state-of-art ASTs as a basis for studying the effect of single degradation mechanisms on performance under real operating conditions.

The deliverable D4.2 aims to identify the effect of the single degradation mechanisms on each specific MEA component. In addition, new AST protocols have been developed and validated to reproduce faster the real ageing profile observed under specific operation. The development of these protocols derives from ageing tests from real system as well as ageing tests representative of the real world performed in single-cell hardware. The information gained from these tests and the synergic combination of modelling activities and ex-situ characterisation contributed to the analysis of the degradation mechanisms. To ensure the harmonization of the results, the specific protocols are developed to be used on the new reference hardware.

In addition, the deliverable gives, and overview of the main stressors related to each specific single degradation mechanisms to assess the impact at different operating conditions and propose a transfer function from AST to single-cell.

In Section 2 of the document are presented the ASTs available for each component and experimental approach is discussed. In sections 3 and 4, the effects of the single degradation mechanisms related to the catalyst layer and the membrane are presented while in section 5 the degradation mechanisms and ASTs of the GDL are discussed. Section 6 describes the new accelerated protocol developed to reproduce the real start-up mechanism, in addition with a systematic analysis of the main stressors.

2. Characterization protocols for zero-gradient Fuel Cell

The definition of suitable operating conditions for performance characterization that, coupled with the zero-gradient Fuel cell, permit to evaluate the performance of MEA components and analyse the occurrence of specific degradation mechanisms during ASTs. The definition of conditions for polarization curves started from the analysis of ID-FAST driving cycle as well as the testing protocol defined for stack. The operating conditions were designed with a double purpose: to predict the local behaviour of full-scale cell, through the use of the reference single cell in order to compare ASTs degradation and real-world operation (*i.e.* driving cycle operation); to standardize performance characterization of different components during aging, under different operating conditions. This also implies the possibility to obtain sufficient data to build and use the transfer functions that correlates testing in single cell and real operation in stack. Below the steps which have led to the design of specific polarization curves are elucidated.

To account the heterogeneities that typically occurs in a full-scale cell, it was agreed to consider two sets of operating conditions, the purpose of which is to represent the “INLET” and the “OUTLET” zones,

since they are considered from aged data available from previous project as the most stressed during operation. Cathode outlet operating conditions depend in general on the specific hardware adopted and are not predictable *a priori*. So, they were obtained applying mass balances on every single point of the driving cycles. In summary, the testing conditions to be adopted in reference single cell were discussed and a unique definition of test procedures was proposed. To define a comprehensive dataset for materials performance under different operating conditions and to ensure comparability according to the “EU-Harmonization” activity coordinated by JRC¹, some specific polarization curves under specific test conditions were defined, considering cathode inlet and outlet at both hot and cold conditions. Please note that the “CatInCOLD” conditions are equivalent to the ID-FAST condition for stacks. They consist in the following module, as depicted in Table 1, to be performed in sequence:

Table 1 – Polarization curve operating conditions for MEA characterization in zero-gradient Fuel Cell.

Code	T.Si. CL / °C	DPT. Si.C / °C	T.Si. .C / °C	DPT. Si.A / °C	T.Si. .A / °C	RH.S i.C / %	RH.S i.A / %	p.Si .C / kPa abs	p.Si .A / kPa abs	Conc.Si. C.O ₂ / %	Conc.Si. A.H ₂ / %
P - Reference	80	80	85	80	85	100	100	230	250	20.9	100
A - CatInCOLD/I DFAST	68	43	73	58	73	30	63.5	280	300	20.9	100
B - Oxygen	68	68	73	68	73	100	100	280	300	20.9	100
C - CatOutCOLD	68	68	73	53	73	100	50	140	190	20.9	100
D - EUHarm	80	80	85	80	85	100	100	230	250	20.9	100
E - CatInHOT	85	57	90	85	90	30	100	280	300	20.9	100
F - CatOutHOT	95	88	95	72	95	77	40	280	300	20.9	100

In the third sections the effects of single degradation mechanisms are studied separately for the catalyst layer, the carbon support and the membrane adopting DoE AST protocols. The description of the protocols is summarised in Table 2.

¹ Tsotridis, G., Pilenga, A., Marco, G. De, & Malkow, T. (2015). EU Harmonised Test Protocols for PEMFC MEA Testing in Single Cell Configuration for Automotive Applications; JRC Science for Policy report. <https://doi.org/10.2790/54653>

Table 2 - Operating conditions of Accelerated Stress Tests

	Catalyst Support AST	Electrocatalyst AST	MEA Chemical AST
Wave form	Triangle square wave	Square wave cycle	-
Upper/Lower potential limit	1.5 V/1.0 V vs RHE	0.6 V/0.95 V vs RHE	OCV
Scan rate	0.5 V s ⁻¹	0.7 V s ⁻¹	Steady-state
Cycle time	2 s	6 s	-
Cell temperature	80 °C (30°C where indicated)	80 °C	90°C
Relative humidity	100%	100%	30%
Outlet pressure	Atmospheric	Atmospheric	150 kPa (abs)
Anode/cathode gas	H ₂ /N ₂ at 0.06/0.06 NI min ⁻¹	H ₂ /N ₂ at 0.06/0.06 NI min ⁻¹	H ₂ /air at stoichiometries of 10/10 at 0.2 A/cm ² equivalent flow

Prior to testing, MEAs were conditioned using a galvanostatic procedure as defined in ID-FAST endurance test program (H₂/air flows fixed stoichiometry anode/cathode = 2/4 at 65°C, 100% relative humidity (RH), ambient pressure): 0.5 A/cm² for 60 min, 2 min at 0.2 A/cm², and 2 min at 0.8 A/cm². This sequence was repeated 10 times, after which constant performance was reached. For performance characterization polarization curves were recorded in galvanostatic mode at Beginning of Test (BoT) and End of Test (EoT). The ORR kinetics (*i.e.* mass activity and Tafel slopes) were determined from oxygen polarization curve, after application of corrections for: ohmic voltage drop (*iR*-free), determined by Electrochemical Impedance Spectroscopy (EIS) measurement of High Frequency Resistance (HFR) at a specific current density; membrane short-circuit and hydrogen crossover, were determined by Linear Sweep Voltammetry (LSV). Cyclic voltammogram (CV) were recorded at cathode electrode at each stop (H₂/N₂ flow rate 60 mL/min at 30°C, 100% relative humidity (RH), ambient pressure) and Electrochemical Active Surface Area (ECSA) was calculated integrating H-desorption charge (using a specific charge of 210 μC/cm²_{Pt}) and averaging over 5 voltammograms. The Oxygen mass transport resistance (R_T) was calculated from limiting current measurements at 80°C and 100% RH under fixed flow conditions (2 NI/min of H₂ and 4 NI/min of O₂/N₂ mixtures).

Specific modifications introduced in the protocol, to characterize the materials, are discussed in the individual sections.

Description of Zero-P reference hardware

A novel zero-gradient cell Fuel Cell has been appositely developed at Politecnico di Milano to operate the MEA in homogeneous conditions over the cell area.

One of the most crucial characteristics is the pattern of the gas channels, as shown in Figure 1: a parallel flow design was chosen as it is the one that minimizes the pressure drops. Despite, this type of flow field is not optimal for gas distribution and water management, these drawbacks have been overcome by the effects of the high stoichiometric ratios utilized (*i.e.* anode/cathode = 8/10). A parallel channel design was adopted to minimize pressure drops, permitting to adopt high reactants stoichiometry to homogenize gas and water distribution. The configuration featuring small-channels (24 channels 0.4 mm x 0.6 mm at cathode, 25 channels 0.3 mm x 0.3 mm at anode) and large-ribs (0.25 mm at cathode, 0.55 mm at anode), with similar performance as observed for the JRC reference zero-gradient hardware², to homogenize the gas distribution over the active area of the CCM. Temperature distribution is collected at both anode and cathode graphite-plate. A liquid-cooling system was introduced to guarantee uniform temperature distribution. While the total width of the channels (20 mm) was imposed by the desired active area, their length (123.5 mm at cathode and 96 mm at anode) was chosen to be significantly longer than of the MEA to assure a complete pre-heating and flow development prior to the gas reaching the GDL. In addition, two large manifolds both at the inlet and outlet were designed to ensure a uniform gas distribution in all the channels.

Zero-P hardware performance has been checked. By adopting the JMFC MEA, the results of the different polarization curves operating conditions, as reported in Table 1, are collected in Figure 1(B).

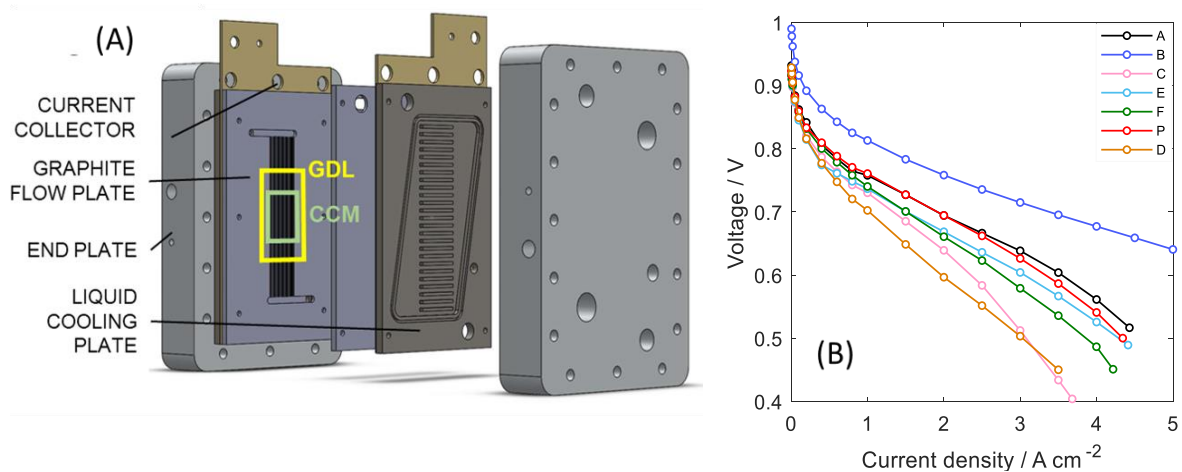


Figure 1 - Zero-gradient Fuel Cell setup designed to operate the MEA in homogenous conditions over the cell area (10 cm²); (B) Effect of different operating conditions under polarization curve for JMFC MEA, tested on the Zero-P cell.

CFD analysis was performed to evaluate the performance and uniformity of the operating conditions in the zero-P, specifically: current density, temperature, membrane water content. Material properties (thickness, conductivity, catalyst activity) were calibrated on performance

² Bednarek, T., & Tsoitridis, G. (2020). Comparison of experimental data obtained using the reference and the single-serpentine proton exchange membrane single fuel cell testing hardware. *Data in Brief*, 31, 105945. <https://doi.org/10.1016/j.dib.2020.105945>

data available for a material coming from a previous European Project (Second-Act – ID 1084). Resulting polarization curve is reported in Figure 2, which was simulated in the operating conditions suggested by JRC as modified for the new hardware. Effect of relative humidity of air at the inlet was evaluated to estimate the uniformity of the current density distribution over the active area. A deviation below $\pm 2\%$ was demonstrated in all the operating conditions tested.

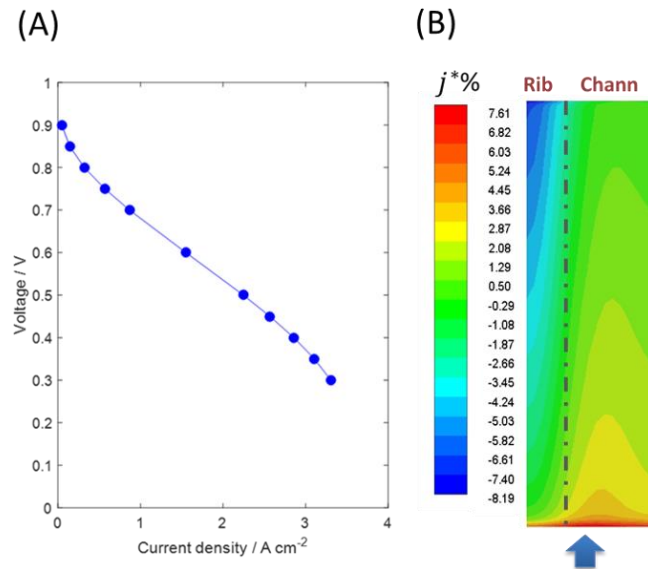


Figure 2 - (A) Simulated polarization curve obtained in Ansys Fluent. (B) Current density distribution over the active area simulated at 0.4 V (equal to 2.86 A/cm²)

To evaluate the impact of geometry and configuration a sensitivity analysis was performed:

- Effect of the flow configurations, *i.e.* co-flow and counter-flow
- Effect of single channel geometry modifications because of manufacturing errors, within 50 μm , on both cathodic and anodic sides.

For what concerns the flow configuration, it was evaluated under the operating conditions, reported above in the case with 100%/30% relative humidity at anode and cathode inlet. It was found that the average current density was not affected by the change in flow configuration: simulated current density was 2.862 A/cm² in both cases. Minor differences were detected in co-flow versus counter-flow configuration.

Further analysis was carried out to evaluate tolerance in the manufacturing process. A simulation was performed to evaluate the presence of a single channel with a larger width (+50 μm) at anode (CASE1) and cathode (CASE2). Same pressure difference between inlet and outlet was applied to the channel, to quantify the stoichiometry value resulting from this new condition. Results are reported in Table 3. The variation of average current density was estimated in -2.5% in the worst case (CASE2), where air stoichiometry was found to change from 10 to 11.2. This value is evaluated as acceptable.

Table 3 - Analysis of manufacturing errors on the average current density as obtained from CFD analysis.

	Base case	Case 1	Case 2
Inlet Stoichiometry A / C	8 / 10	10.6 / 10	8 / 11.2
Current density [$A\ cm^{-2}$]	2.862	2.843 (-0.6%)	2.790 (-2.5%)
Voltage [V]	0.408	0.408	0.408

Looking at local distribution of current density, against the reference case, it was found that differences are very limited for CASE1, since hydrogen diffusion coefficient is higher than oxygen. In CASE2 the lower rib size induced a less uniform distribution of water in the porous media which explained the observed difference in current density, still acceptable in the light of the current analysis.

3. State of Art analysis of AST and identification of necessary improvements

A wide and comprehensive analysis of the major degradation mechanisms occurring in PEMFC during automotive operation and the most diffused AST's to reproduce them was carried out by the whole Consortium, with the contribution of the Advisory Board, especially during the 1st Workshop organized in Nantes in February 2019.

The following table summarizes the major results of such analysis, identifying 4 AST's on which ID-FAST activities will focus to provide improved protocols that will be the basis to develop the combined AST (cf. public deliverable D4.3 "Analysis of coupling between mechanisms and definition of combined AST").

Table 4 - Description of single degradation mechanism and SoA AST protocols.

AST	Mechanisms	Reference AST	Improvement	Indexes (Measurement technique)
Cathode activity loss	PGM dissolution and ripening	DOE, IEC, JARI Consolidated, but effect of stressors not fully investigated	Potential limits, slow rate, wave form and flow rate	<ul style="list-style-type: none"> • Mass activity • ECSA loss (CV) • mass transport R (limiting i) • ionomer conductivity (EIS)

Cathode Catalyst support degradation	Carbon corrosion	DOE, IEC, JARI Consolidated, but effect of stressors not fully investigated	Based on potential cycling based on simulated start-up	<ul style="list-style-type: none"> • Mass activity • ECSA loss (CV) • mass transport R (limiting i) • ionomer conductivity (EIS)
Porous layers degradation	Hydrophobicity loss, mechanical ageing	Ex-situ not harmonised	In-situ AST	Not defined
Bi-polar plates degradation	Corrosion	Ex-situ not harmonised	Ex-situ and in-situ	Not defined

To assess the impact on the performance of the single-degradation mechanisms, state-of-art AST protocols have been applied on the reference MEA. The main objective of this activity is: clarify the effect on the performance indices as expressed in Table 4 of the single degrade and apply these indices to case studies of real functioning such as the driving cycle protocol and off-specific events such as start-up / shut- down operation.

Electrocatalyst AST

Voltage sweep in H_2/N_2 are commonly imposed to accelerate the electrocatalyst degradation at cathode electrode. The main phenomenon occurring is Pt dissolution that causes the agglomeration of Pt particles, mainly due to Ostwald ripening, and the migration within the membrane. Data collected in this section will be used to discriminate which degradation mechanism prevails under start-up/shut-down cycling. Emphasis will be posed on the evaluation of kinetics losses. The test was performed on JMFC MEA and Freudenberg GDL following the protocol described in Table 2.

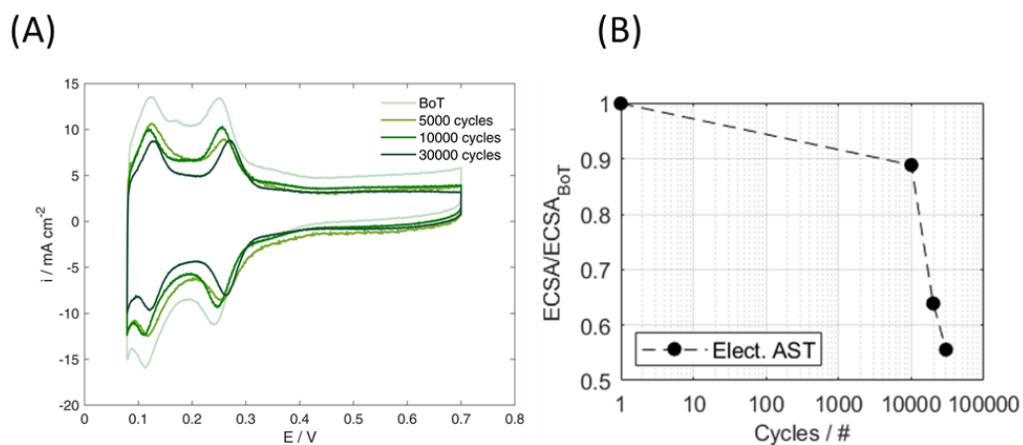


Figure 3 - CV measured during electrocatalyst AST at 30°C, 100% RH, P ambient. (A) Cyclic voltammogram; (B) Relative ECSA.

The evolution of CV profile as depicted in Figure 3 during ageing, the reduction of ECSA value was about 45%.

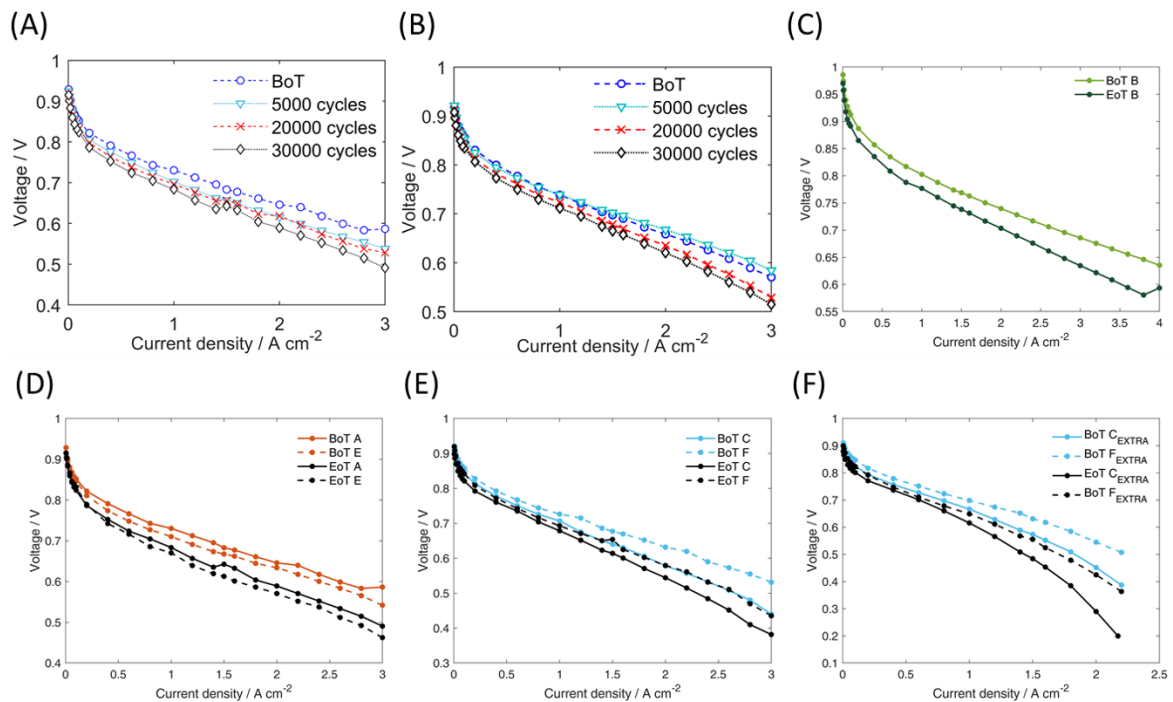


Figure 4 - Analysis of performance evolution during electrocatalyst AST for JM CCM and Freudenberg GDL at different operating condition as described in Table 4. (A) ID-FAST curve, (B) reference curve, (C) oxygen curve, (D) cathode inlet at condition low power / A versus high power / E, (E) cathode outlet at condition low power / C versus high power / F, (F) 10% oxygen concentration effect at cathode outlet at condition low power / C versus high power / F.

The complete set of polarization curve as depicted in Figure 4. In both ID-FAST (*i.e.* cathode in – low power) and reference polarization curve (Figure 4 (A-B)) the degradation causes a vertical translation of the curve between BoT and EoT, even if degradation is slightly more pronounced in high current region. Similar trend was confirmed testing cathode inlet, both at low and high-power operating conditions, as shown in Figure 4 (D). The ECSA loss calculated correspond to a theoretical voltage loss of 26 mV. Thus, the mean change in oxygen polarization curve correspond to -36 mV, that is in quite good agreement with the prediction based on ECSA measurement. Analysing the trend of the oxygen polarization curve (see Figure 4(C)), the reduction of mass activity (-50%) is then consistent with the ECSA reduction.

The effects of Pt dissolution in cathode outlet section are comparable at low or high load as well (see Figure 4(E)). The MEA performance seems degraded homogeneously in the two conditions: a vertical shift can be recognized at low current density and the ohmic losses increase as well. The reduction of membrane proton conductivity and the reduction of reactants diffusivity compromise the mass transport region with a double of voltage losses. Probably, ECSA reduction leads to an increase of local fluxes at catalyst sites, and this is visible in the mass transport region particularly at cathode outlet, that represents a critical operation. The effects on the performance of the reduction of the diffusivity

of reactants are stressed in polarization curve with diluted air Figure 4(F): the two curves show a strong reduction in the limiting current region and a slight increase of activation losses.

Carbon support AST

The catalyst support protocol uses a rapid triangle wave cycle to accelerate the corrosion of the catalyst support minimizing the degradation of the catalyst itself. The potential range of the protocol is similar to un-mitigated start-up or shut-down. Carbon Support AST forces the mechanism of carbon oxidation, which led after several cycle at the electrode collapse³. The porosity and the tortuosity of the carbon texture change, the gas transport resistance increases, and the triple phase boundary of the electrode gets worse because of Pt nanoparticles detaching.

The evolution of the cyclic voltammetry profile and ECSA, at different AST stops are reported in Figure 5.

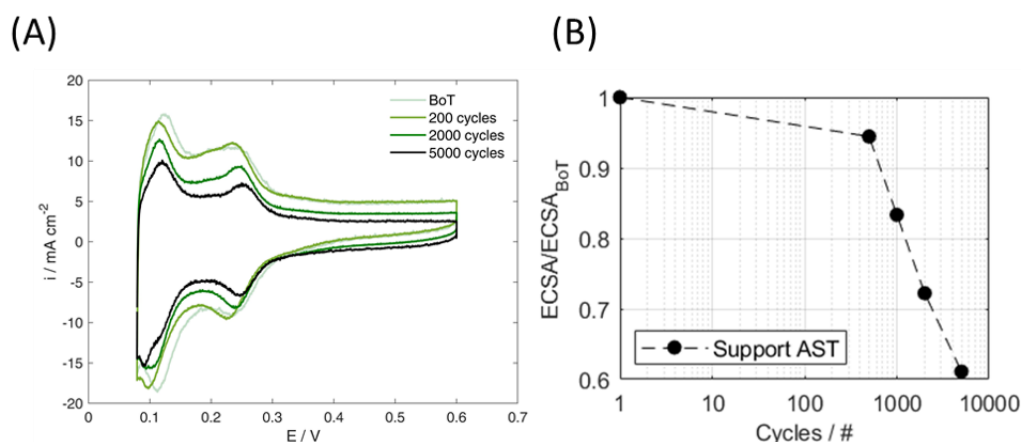


Figure 5 - CV measured during support AST at 30°C, 100% RH, P ambient. (A) Cyclic voltammogram; (B) Relative ECSA.

Performance loss induced by voltage cycling are evaluated in Figure 6. H_2/air polarization curves were performed and the results at BoT and at each stop are reported in, for the reference and the ID-FAST operating conditions (see Figure 6(A-B)). In both cases in the first 1k cycles MEA performance slightly increase probably because the break-in procedure does not guarantee a complete activation of the MEA, or few cycles at high potential have a beneficial effect on cleaning of the cathode electrode. After 2000 cycles, the effects of degradation are visible: significant ohmic and mass transport losses can be recognised by the i - V curves. The kinetic performance loss due to platinum dissolution can be estimated based on the decrease of catalyst surface area. After 5000 cycles at high voltage, the theoretical voltage loss is -31 mV. In experimental results obtained in Reference, ID-FAST and Oxygen

³ Schulenburg, H., Schwanitz, B., Linse, N., Scherer, G. G., Wokaun, A., Krbanjevic, J., Grothausmann, R., & Manke, I. (2011). 3D Imaging of Catalyst Support Corrosion in Polymer Electrolyte Fuel Cells. *The Journal of Physical Chemistry C*, 115(29), 14236–14243. <https://doi.org/10.1021/jp203016u>

polarization curves are respectively: -112 mV, -53 mV and -75 mV at 1.5 A/cm². These values are higher compared to the theoretical one, suggesting that also worsening of proton and oxygen transport are involved. Cathode inlet operating conditions at low and high power are reported in Figure 6(D). The reduction of performance is visible in both tests with a similar end-of-life result between the low and high-power case. The loss of performance is respectively -53 mV and -46 mV at 1.5 A/cm². In the cathode inlet conditions, a more contained loss of performance is observed compared to the reference case, probably linked to the low RH value at the cathode and a consequent greater partial pressure of oxygen. This effect is visible in particular at high current density, *i.e.* above 2 A/cm².

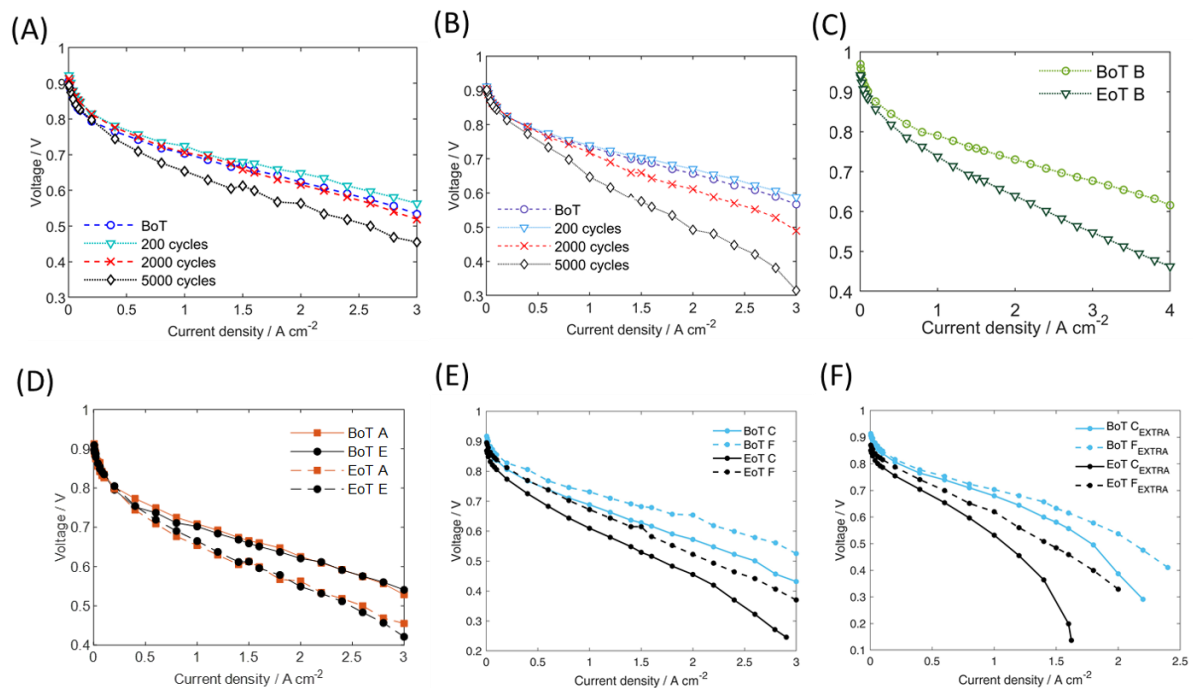


Figure 6 - Analysis of performance evolution during catalyst support AST performed at 80°C, for JM CCM and Freudenberg GDL at different operating condition as described in Table 2. (A) ID-FAST curve, (B) reference curve, (C) oxygen curve, (D) cathode inlet at condition low power / A versus high power / E, (E) cathode outlet at condition low power / C versus high power / F, (F) 10% oxygen concentration effect at cathode outlet at condition low power / C versus high power / F.

The effects of carbon corrosion in cathode outlet section, as depicted in Figure 6(E), are comparable at low or high-power condition. A vertical shift can be recognized at low current density and the ohmic losses increases at medium/high current densities. The reduction of membrane proton conductivity was confirmed by HFR, measured in EIS. The slope of the polarization curve increases slightly in middle region, but mass transport losses become relevant above 2 A/cm². The effect of the increase of oxygen transport resistance was stressed in diluted air polarization curve, depicted in Figure 6(F). The results at the end of the test show a heavy reduction of the limiting current and a slight increase of activation losses. At both BoT and EoT, these two tests are characterized by higher oxygen transport resistance (R_T) caused by the lower oxygen partial pressure, but this effect is more pronounced in Polarization C_{extra} at lower operating temperature.

Membrane AST

Many factors contribute to the chemical decomposition of PEMs including reactant gas cross-over, radical formation, Pt dissolution and redeposition, and transition metal ion contaminants. Peroxyl (OOH*) and hydroxyl (OH*) radical attack on the remaining H-containing terminal bonds on polymer end and side chains is commonly believed to be the primary degradation mechanism. The effects of the formation of radicals are mainly driven by OCV steady state of the cell with air feeding. Moreover, the membrane is mechanically stressed: high temperature and low relative humidity are imposed to point thermal non-humidification stress. The combination of high operating temperature and low relative humidity stress the possible mechanical degradation of the membrane increasing the possibility of cracks and tears caused by local stresses. To avoid irreversible damage, AST is carried out for 350 h with intermediate recovery step.

The open circuit voltage is not a selective measure method but provides an indication of the membrane condition and can be correlated to the fluoride release rate. Stabilized MEA's show a basically constant OCV and negligible fluoride emission. During AST occurring the reduction of OCV is the clearest indicator used to quantify the degradation occurrence and its effects on cell performance.

The OCV trend is depicted in Figure 7(A).

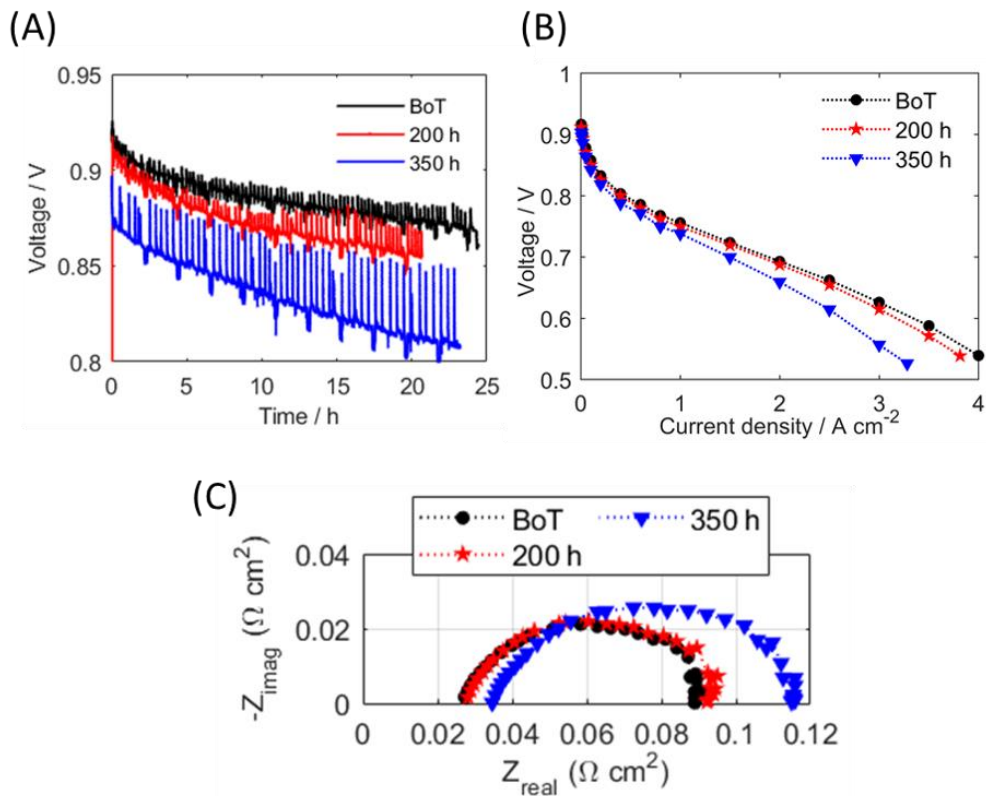


Figure 7 - (A) OCV change during AST membrane cycling. (B) Polarization P during membrane AST cycling. (C) EIS performed at 2 A/cm².



The distribution of OCV decreases monotonously during the test. Each step increase is affected by degradation as well: after each stop initial OCV value is lower.

The increase of OCV at different anode/cathode pressure measured does not show any decrease of cell voltage when the anode is pressurized from 150 kPa to 170 kPa: this indicates the absence of pin hole formation in the membrane. The OCV increases with the increase of pressure. The reduction rate of OCV increases with cycling hours: this stands for the gradual increase of degradation effects. This conclusion is confirmed by the evolution of the polarization curve, as shown in the Figure 7(B).

High Frequency Resistance changes as result of degradation, as visible in Figure 7(C). The value of HFR is mainly affected by the mechanism of degradation. Chemical effects result in the reduction of proton conductivity and thickness: the reduction of thickness and proton conductivity compensate possible change of the resistance. In this perspective, HFR changes are visible after 350 hours of cycling. The change of the shape of the charge transfer resistance (R_{CT}) suggests an increase of activation losses at anode and cathode side based on the possible reduction of the catalyst active area. In Nyquist plot during the first 200h any change can be noticed: the curve does not present any visible effects in performance. The degradation of the cell mainly affects the mass transport zone and the ohmic section. The increase of ohmic effects is the results of the loss of membrane proton conductivity: cross-over compromises the performance of the cell at intermediate value of current density.

The degradation effects of the AST cycling are mainly localized in ohmic losses zone where the performance of the membrane is the most effective factor: limiting current resistance should not change and the limiting current as well. To confirm the results oxygen transport resistance was measured and no change was highlighted.

4. Analysis of stressors in catalyst layer degradation

Activities conducted in this frame at CEA were based on the state of the art previously described and focused on the degradation of the cathode catalyst layer. The final aim is the integration of most relevant stressing factors within relevant combined operando ASTs. To this end, the investigations presented here are dedicated to the development of protocols, taking into account the phenomena and mechanisms addressed by SoA ASTs to degrade the catalyst, but looking for tests applicable into real PEMFC conditions (mainly H_2 /Air), whereas the SoA tests are applied in-situ but not operando (namely under H_2/N_2).

The approach was to first mimic the basic principle of these ASTs, *e.g.* to create voltage cycles as first stressor parameter and then to extend the study towards operating conditions and specific additional events, always targeting to enhance the degradation of the catalyst and check the related performance losses.

Several protocols have been defined based on actual PEMFC Hydrogen and air operation:

- with basically two steps load cycles inducing close to a square wave voltage protocol;
- considering different dwell time for the current steps (as considered during the development of H_2/N_2 ASTs);

- looking at the impact of relative humidity as one of the most impacting operating conditions;
- increasing the time at higher voltage with open circuit voltage steps;
- adding start and stop events, including H₂/air front at restart to intensify Pt dissolution and carbon corrosion and always check the actual impact onto the degradation rates.

Description of the protocols

The US/DoE protocol considered is the AST cycle for catalyst degradation following a potential square waves profile 0.6V/ 0.95V with steps of 3s / 3s, applied at 80°C under humidified H₂/N₂.

To build the protocol, first step was to define the load cycles to be in the same voltage range, based on the polarization curve obtained at beginning of life in appropriate operating conditions (Figure 8). An additional constraint had to be taken into account: the need to define a clearly measurable lower current enabling to measure a maximum voltage, not too close to the OCV.

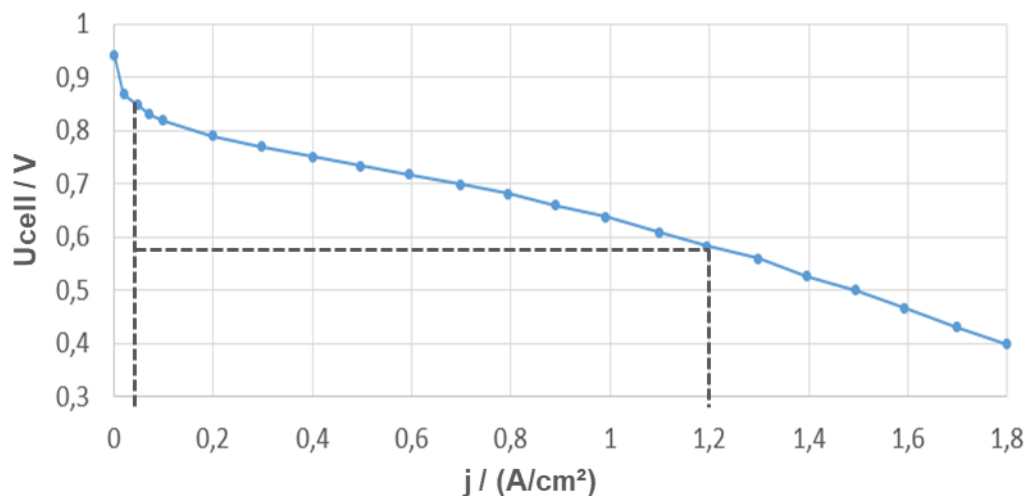


Figure 8: initial polarisation curves obtained with the reference ID-FAST MEA components in the 25 cm² CEA serpentine single cell. H₂/air - 80°C, 1.5 bar abs, HR 50/50%, Stoich. 1.5/2.

The best suited equivalent current densities for AST under H₂/Air were thus the following (Figure 9): 30 A (=1.2 A/cm²) / 1 A (=0.05 A/cm²) corresponding to 0.58 V / 0.8 V at BoL. Dwell time of each current steps were fixed at 6 seconds for this initial reference case to be close the duration of SoA cycles but allowing to properly control and record voltage data.

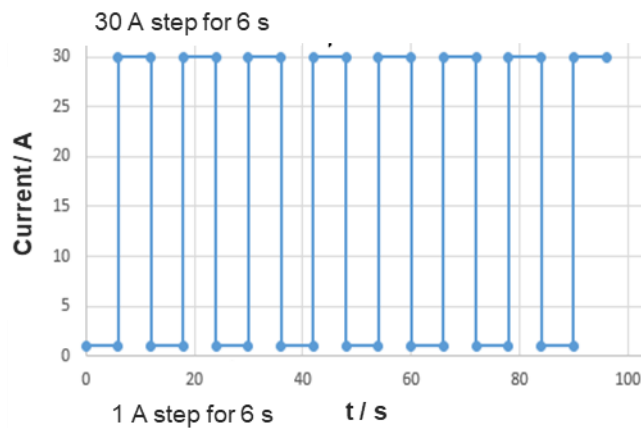


Figure 9: two steps load cycles 1A/30A – 6s/6s.

An OCV step has then been added to increase cathode potential (to get closer to 0.95 V) and promote oxidation mechanisms enhanced at higher voltage (Figure 10).

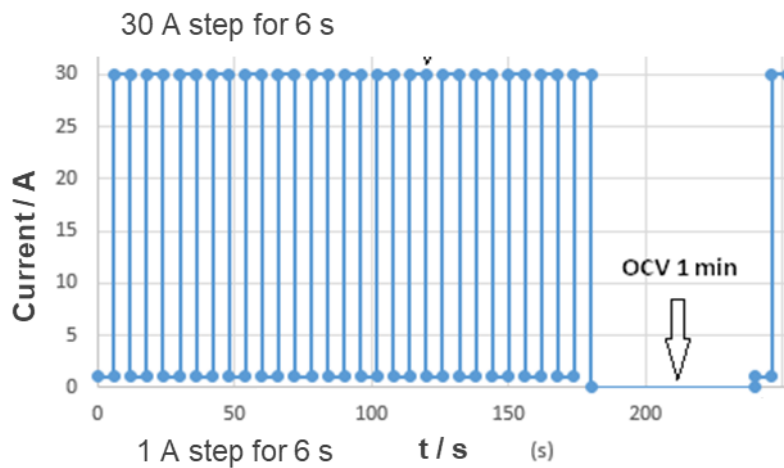


Figure 10: two-steps load cycles 1A/30A – 6s/6s with an OCV step of 60 seconds added after 180 seconds (25% of time).

A slightly different load profile (Figure 11) has also been proposed reproducing same two-steps load cycles of 6s/6s with 25% of time under OCV but with shorter OCV periods to check the relative impact of steps and overall time a higher potential.

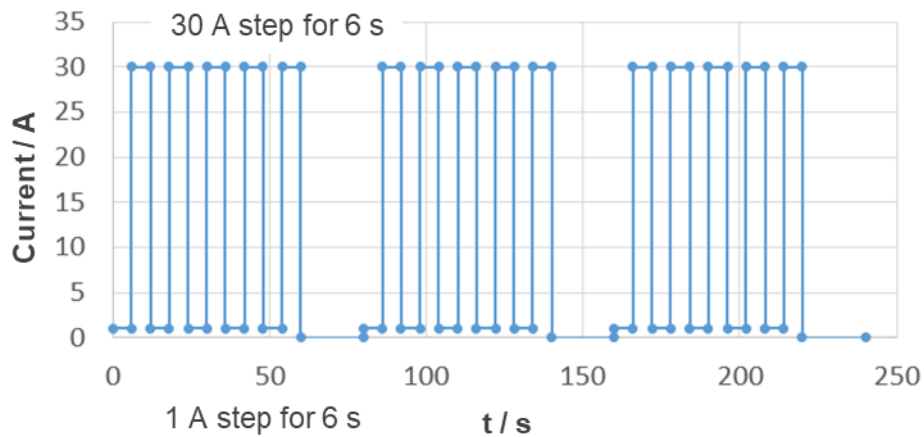


Figure 11: two-steps load cycles 1A/30A – 6s/6s with three OCV steps of 20 seconds added after 60 seconds of cycles (25% of time).

In order to particularly consider the effect of time regarding formation and reduction of the oxides and the possible impact induced onto performance or catalyst degradation, dwell time has been doubled for a third two-step current AST type (Figure 12), bearing in mind the ranges explored for the development of SoA ASTs.

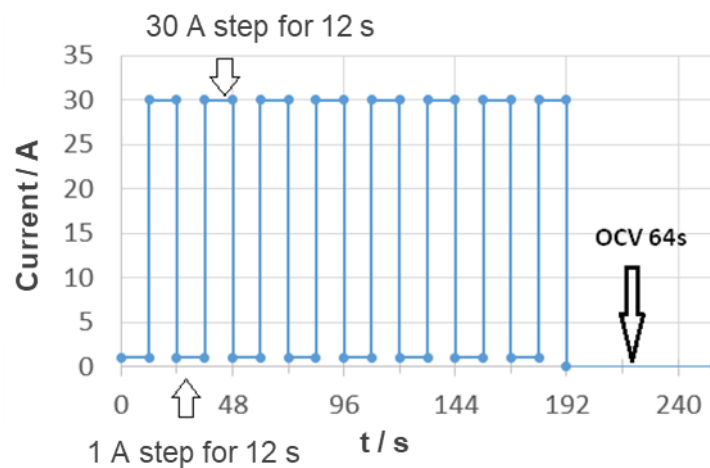


Figure 12: two-steps load cycles 1A/30A – 12s/12s with an OCV step of 64 seconds added after 192 seconds (25% of time).

A last type of ageing event has been introduced to simulate harsh shut-down and start-up events including the creation of a hydrogen / air front anode side at high temperature (not cooling to ambient but controlled at 60°C). These SU/SD events are added each 24 hours within the two-steps load cycles 1A/30A of 6s/6s.

The procedure is conducted to decrease the overall pressure before feeding the anode with nitrogen, and then waiting for the air to diffuse from the cathode into the anode. The device and protocol



allowed to apply variable flows. First, the flowrates of H₂ and Air are reduced to the minimum (equivalent to 5 A, or a current density of 0.2 A / cm²). Then H₂ is stopped and replaced by N₂ while the cell temperature is reduced to 60°C, bubblers remaining at 64°C. The decrease in temperature is much slower than the time required for the oxygen to diffuse into the anode. The cell voltage drops close to 0 V. Meanwhile, for 10 min, the cathode is supplied with air while the nitrogen is stopped anode side. After this period, the hydrogen is injected again into the cell until the OCV is reached, and the load applied again until the temperature reaches 80°C again.

As for the operating conditions, fixed flow-rates corresponding to the maximum current during cycles were selected to avoid any pressure peak or drop due to possible issues with test bench regulation e.g. stoichiometric ratios of 1.5 and 2 at 30A for respectively Hydrogen and Air. Other conditions have been selected firstly based on nominal operating conditions applied with the same MEAs during actual drive cycles, e.g. a cell temperature of 80°C with an absolute pressure of 1.5 bars and a relative humidity 50% both sides. Then, the impact of humidity, recognized as a parameter improving the degradation mechanisms affecting the catalyst material, has been checked by increasing the relative humidity to 80% RH both sides, and then by promoting presence of liquid water with gases humidified at more than 100%.

Finally, to further explore the relative impact of load profiles, presence of events or conditions applied, the overall duration of tests, which was first limited to less than 200 hours has been extended in some cases allowing to check the actual modification of voltage losses and degradation rates on the longer term when relevant.

During the ageing tests, diagnostics are applied regularly, namely polarisation curves and cyclic voltammetry to assess the overall losses in performance and electrochemical properties, mainly cathode electrochemical active surface area.

Results and discussion

Experiments have been conducted with a single serpentine 25 cm² single cell and reference components defined for the project ID-FAST: a JMFC CCM based on the developments of other FCH-JU projects for automotive application and a H24C5 GDL provided by Freudenberg (FPM).

Results analysed to compare the impact of the different load profiles and conditions include: the evolution of voltage versus time and overall degradation rates calculated at the two or three currents applied (1A, 30A or 0A); the polarisation curves enabling to assess the non-reversible degradation rates (H₂/Air 80°C, 1.5 bar abs, HR 50/50%, Stoich. 1.5/2) and the cyclic voltammograms (H₂/N₂ 60°C, 1.5 bar abs, HR 50/50%, 200 mV/s) showing the modification of the cathode catalyst and ElectroChemical active Surface Area (ECSA) losses.

First two-steps load cycles 6s/6s

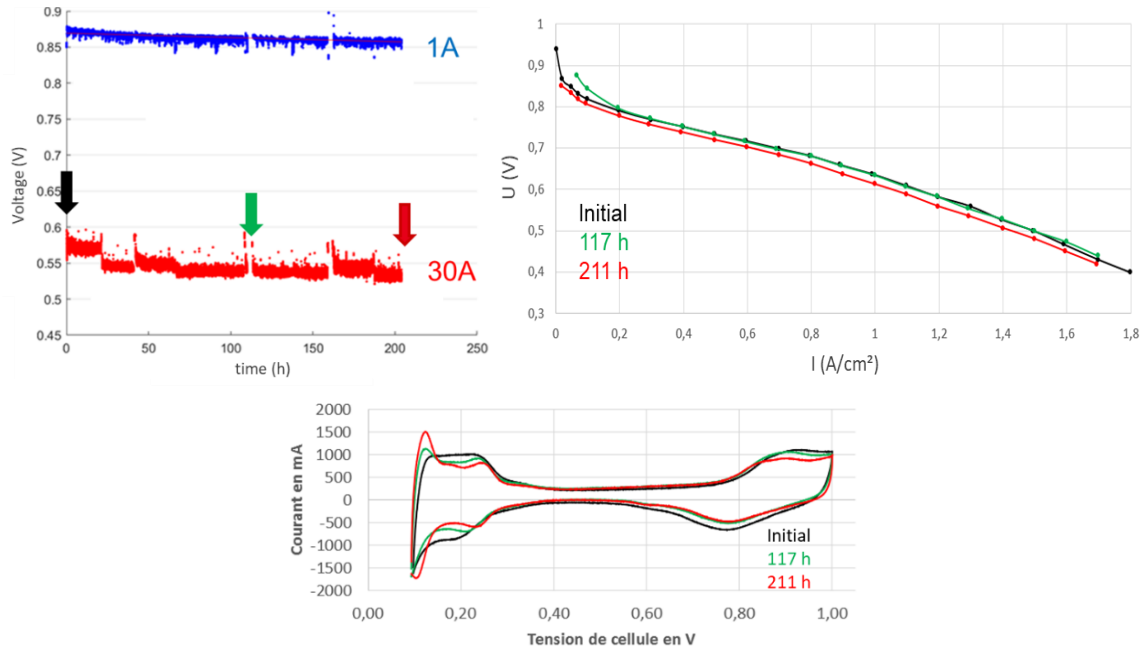
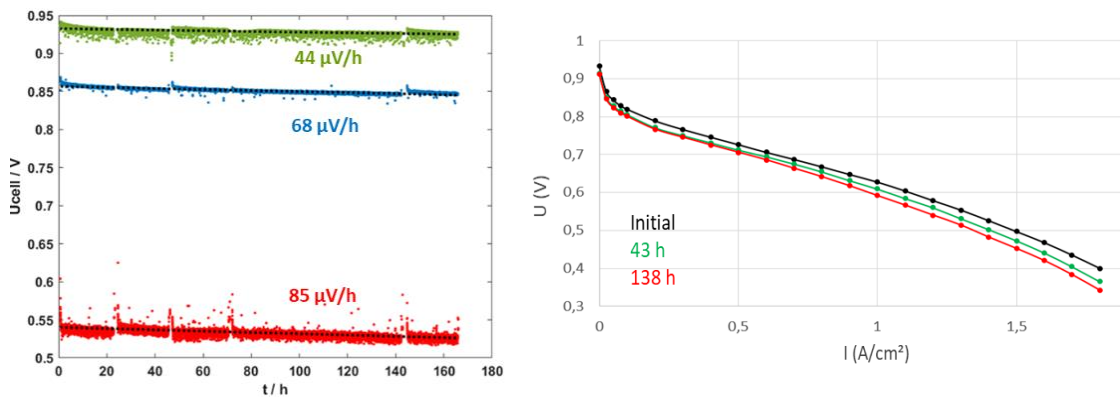


Figure 13: ageing results during two steps load cycles 1A/30A – 6s/6s. Voltage versus time, polarization curves and cyclic voltammograms recorded at beginning of test, after 117h and 211h or end of test).

Degradation rates are high when considering reversible losses, whereas according to polarization curves, the irreversible degradation is low even after 211 h, which correspond to more than 60 000 cycles, e.g. twice the number of cycles considered with the SoA H₂/N₂ protocol. ECSA decreased by only 10%, voltammograms showing small modification of catalyst nanostructure, probably particle growth, maybe slight modification of the carbon support.

These small ECSA and performance losses indicated that these plain two-steps load cycles allowing voltage cycles between 0.6 and 0.85 V were not harsh enough, thus requiring additional stressors to accelerate degradation.

Two-steps load cycles 6s/6s with a 60s OCV step 25% of time



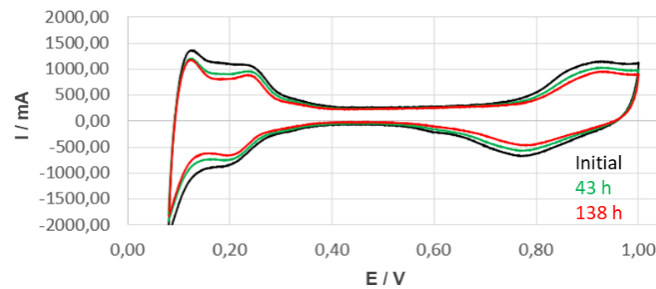


Figure 14: ageing results during two-steps load cycles 1A/30A – 6s/6s + OCV period. Voltage versus time, polarization curves and cyclic voltammograms recorded at beginning of test, after 43 and 138 h or end of test.

When adding one-minute OCV after 3 minutes of load cycles, the degradation rates calculated from polarisation curves are increased by 200% compared to the previous case without OCV. Higher ECSA loss is also observed in this case (40% vs 10%).

It is confirmed that OCV steps induce strong accelerating effect when coupled with load (voltage) cycles and should be integrated as stressor in further combined AST protocols.

In addition, two cases have been compared (Figure 15) showing that for the same AST duration, the longer the OCV step, the higher the ECSA and performance losses.

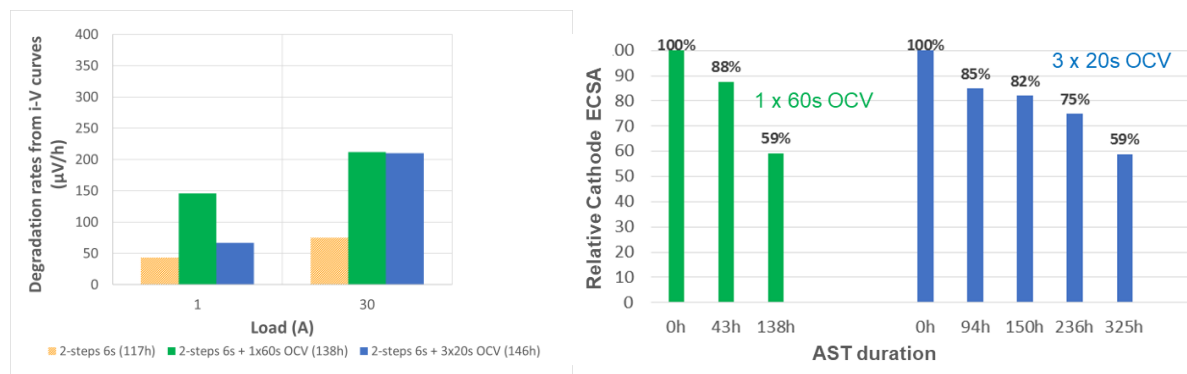


Figure 15: degradation rates from the pol curves (left side) and remaining percentage of cathode ECSA (right side) during the ageing tests conducted in the same conditions with a two-steps load profile of 6s/6s and 25% of time at OCV but with one OCV step of 60s (green) or three OCV steps of 20s (blue).

Two-steps load cycles 6s/6s with a 60s OCV step 25% of time – Effect of RH

A similar experiment was conducted but increasing the relative humidity to 80% for both gases (Figure 16). The main conclusion is that degradation observed was equivalent or only slightly greater. The expected increasing and accelerating effect expected due to higher humidity could have been hindered by slightly better performance reducing the amplitude in voltage between low and high load steps. Conclusion was that actual harsher conditions with more than 100% RH should be imposed to actually accelerate degradation due to this parameter.

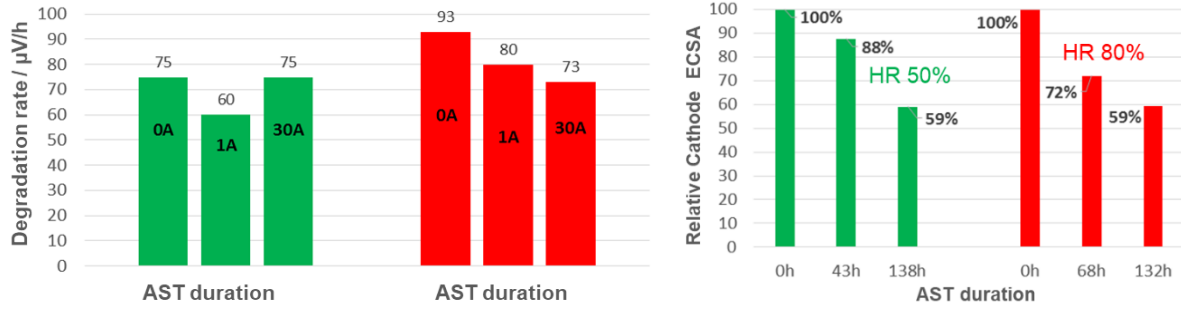


Figure 16: degradation rates (left side) and remaining percentage of cathode ECSA (right side) during the ageing tests conducted following the same load profile two-steps 6s/6s in the same conditions but for gases humidified at 50% (green) or 80% (red).

Two-steps load cycles 12s/12s with a 64s OCV step 25% of time

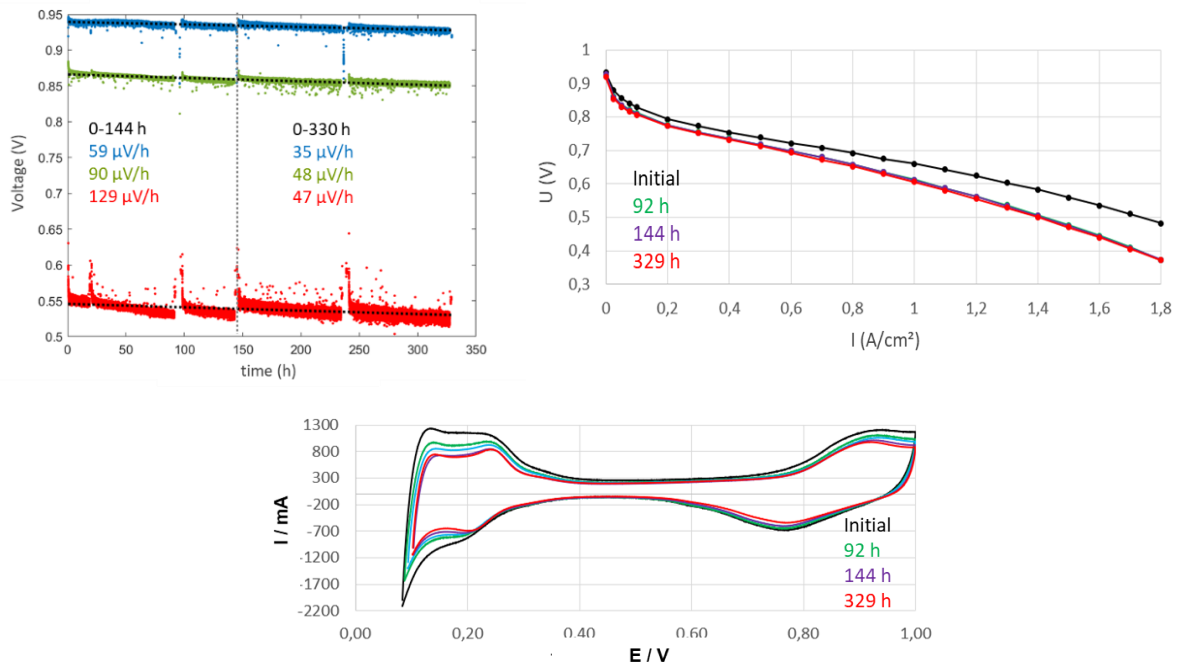


Figure 17: ageing results during two-steps load cycles 1A/30A – 12s/12s + OCV period. Voltage versus time, polarization curves and cyclic voltammograms recorded at beginning of test, after 144h (similar to previous test) and 329h or end of test.

From these data, the difference observed in ECSA and on CV evolution with longer dwell time showed good agreement with performance behavior that is a fast decrease then followed by a « plateau ». Hypotheses are that Pt oxides formation and reduction could be favored by longer steps if kinetics limitation occurred for the shorter steps. It can be mentioned that this observation is different from the literature about SoA AST under H_2/N_2 for which the cycles frequency has been regularly increased

during the development of this protocol. However, it should also be noted that during the SoA catalyst AST, mainly the ECSA loss is analyzed to conclude about the degradation.

This 12s/12s test was conducted on a longer period compared to the previous 6s/6s one allowing to also consider the effect of the number of cycles. Degradation phenomena and rates were thus observed first over a period equivalent in time to the previous test and then for the overall test, with more than double duration but similar number of cycles. After the first period of about 140h, very low extra performance degradation was observed. It could thus be noticed that at least for this range of dwell times (few seconds), the overall duration spent at low and high current (or preferably voltages) had a major impact on the speed of performance loss than the number of steps (or cycles).

When considering histograms of degradation rates for the two tests, the two durations in the second case and ECSA ratio during ageing (Figure 18), it appears that a stabilization is indeed reached by the ECSA even when the ageing is continued for the second test, which is consistent with the fact that performance stop decreasing. However, it can be noticed that there is a delay between the stop in voltage degradation and the stop in ECSA, which occurs afterwards. The interpretation of degradation caused by the AST could be slightly different if only ECSA loss is considered instead of performance loss, which should be kept in mind when defining the combined ASTs and the data analyses of cell performance or MEA properties.

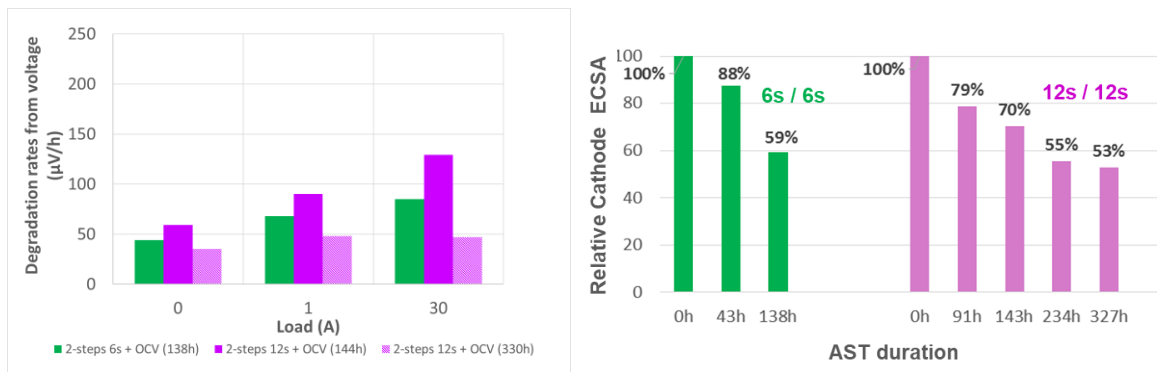


Figure 18: histograms for the two tests with dwell times of 6s or 12s including 25% time an OCV step of about 1 minute. Degradation rates at 0A, 1A and 30A (left hand side), with two ageing durations in the 12s-case and cathode ECSA ratio during ageing (right hand side).

Two-steps load cycles 6s/6s with SU/SD events

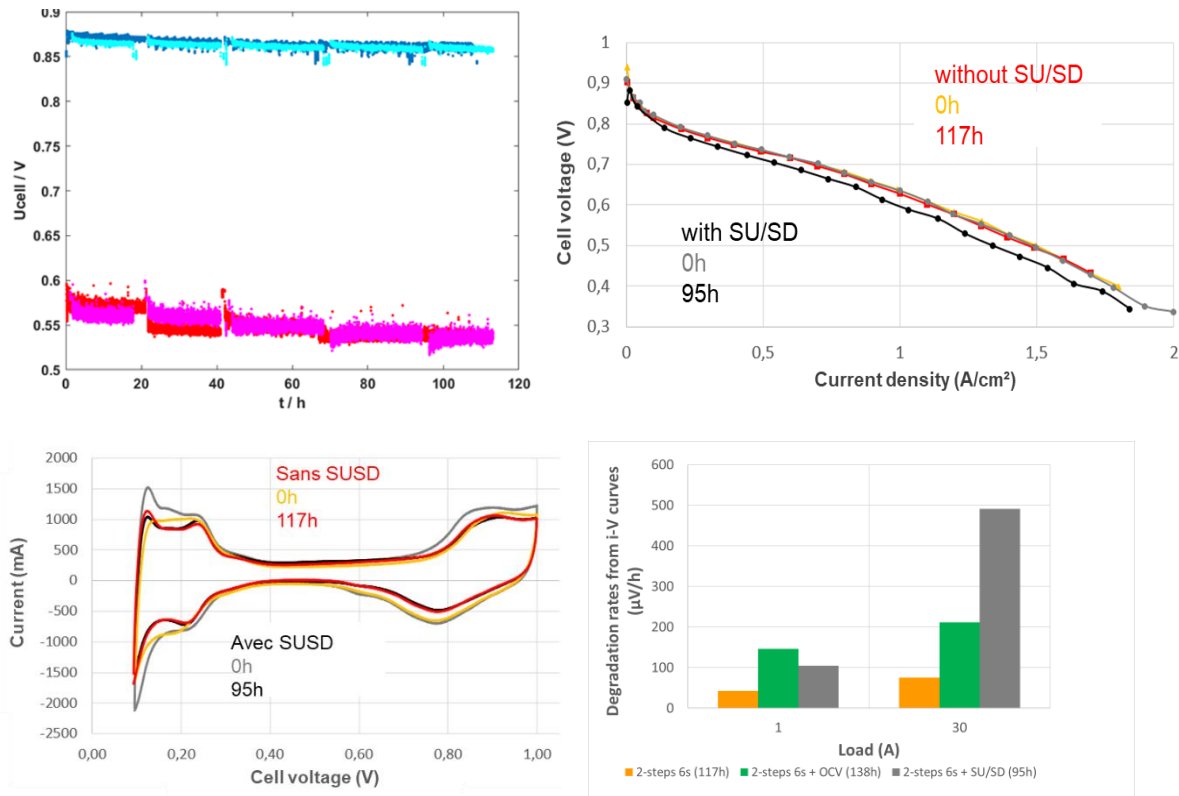


Figure 19: ageing results during two-steps load cycles 1A/30A – 6s/6s with or without SU/SD events. Voltage versus time, polarization curves and cyclic voltammograms recorded at beginning of test and end of test.

From the comparison of voltage and polarisation curves, the SU/SD, with H₂/Air front induced, caused indeed a strong impact more than doubling the degradation rate at high current (low voltage), and showing performance loss on the polarisation curves not observed at all without SU/SD. Cyclic voltammograms show probable modification of the catalyst structure, that will be check by further analyses.

From the degradation rates assessed on the polarisation curves, it appears that OCV and SU/SD events increase the degradation rates similarly at low current and SU/SD has stronger impact at high current.

Conclusions and next steps:

Simple two steps load cycles close to SoA ASTs but under actual PEMFC operation were defined. The possibility to apply AST cycles following this method was confirmed. For the nominal case of two-steps load of 6s each, 100 hours correspond to the 30000 cycles targeted by the SoA catalyst AST. Different experiments were conducted to check the impact of load profiles and operating conditions.

Impact of current step duration (12s/12s vs. 6s/6s) was checked, showing quicker performance losses for the greater dwell time, but not necessarily quicker degradation of the ECSA, showing that both



duration and number of cycles could be important for final selection of stressors and interpretation of results.

Specific OCV periods and harsh SU/SD events with H₂/air front at the anode periodically could be defined and showed actual accelerating impact.

No significant impact of RH increase could be determined for AST over 200 h. Hence increase of RH to more than 100% allowing to inject or condensate liquid water within the cell is considered to actually accelerate degradation with this parameter.

Complement with shorter tests in some cases to confirm acceleration or longer tests, also including increased current range, to compare or fill the gap with real ageing drive cycles, to assess and quantify effect of duration are planned, as well as possible experiments under H₂/N₂ with same cell and MEAs for final validation regarding SoA.

In parallel, post-mortem analyses are performed to check the actual degradation mainly of the cathode catalyst layer microstructure. Conclusions of these AST tests and analyses will be used to integrate appropriate stressors in sequenced and/or combined load cycles ASTs.

5. Development of GDL specific ASTs and effect of stressors

Since no specific operando stressors for the GDL exist, one task by DLR was to study the effect of possible stressors for the GDL and discriminate between their effects on GDL and CCM. Typical stressors such as high cathode potential or RH cycling affects various MEA components in parallel, and identifying a specific stressor, which selectively influences GDL is particularly challenging.

The single cell tests described in this section have been performed using a qCf 25 cm² test cell and the qCf Liquid Cooling high amp single cell hardware (so called zero gradient cell) from balticFuelCells GmbH. The tests have been performed using DLR's in-house developed test stands controlled by programmable logic controllers that allow automatic control of the input and output conditions, such as the pressure, temperature, gas flow rates and humidity. For acquisition of EIS and CV spectra an electrochemical test stations from ZAHNER-elektrik GmbH & Co. KG were used (PP241 potentiostat in a ZAHNER ZENNIUM electrochemical workstation with THALES software).

Before applying a specific AST, the MEAs were first conditioned. Then, the MEAs were characterized by recording polarization curves⁴, impedance spectra and CV. However, in this document, only selected analyses are shown. After BoT characterization the cell was operated under AST conditions. After the completion of AST operation and before performing EoT characterization, the cell was refreshed by a shutdown procedure in order to eliminate reversible degradation effects⁵.

After EoT characterization the cell was disassembled, and the aged CCM as well as GDLs were characterized independently by combining them with corresponding new components to distinguish

⁴ Polarization curves and EIS were recorder under several different RH, T, flow and pressure conditions.

⁵ P. Gazdzicki, J. Mitzel, D. Garcia Sanchez, M. Schulze, and K. A. Friedrich, J. Power Sources, 327, 86 (2016).

between the impact of the stressors on the CCM and the GDL individually. A scheme of this procedure is indicated in Figure 20. The MEAs were composed of CCM from Johnson Matthey and Gore, in addition, GDLs from SGL and FPM. The used material combinations are indicated for each test. The effect on the repeated disassembly and assembly process of the MEA was analysed; the procedure mainly affects the ohmic resistance of the cell which becomes higher upon repeatedly disassembling and assembling of the cell.

The investigated stressors are summarized in Table 5 indicating expected impact on GDL and the in-situ conditions to be applied on the testbench. The following discussion focusses on main observations and follows the order of stressors from the table.

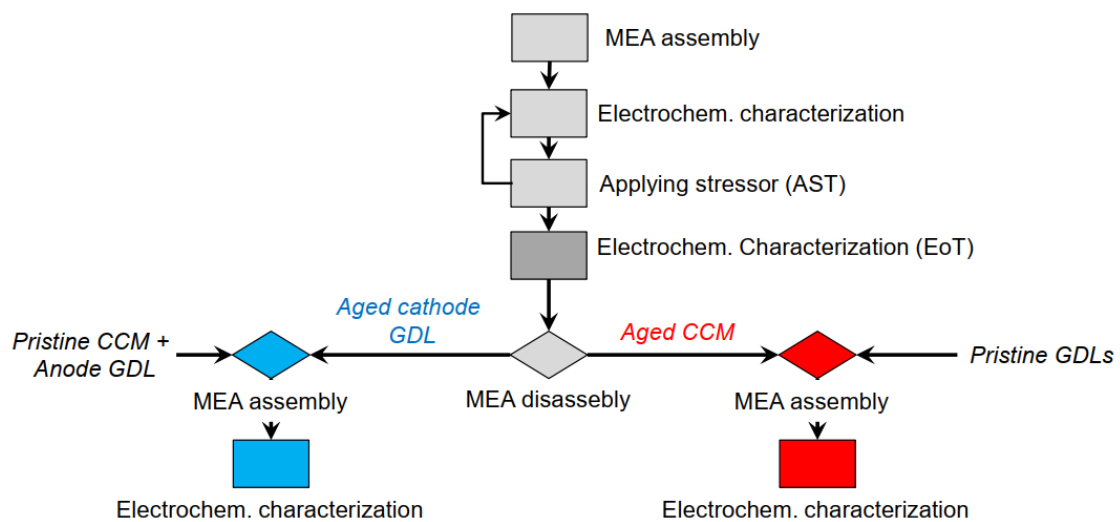


Figure 20: Flow chart to demonstrate the testing approach of possible operando stressors for GDLs.

Table 5: Possible stressors as operando AST for GDL.

Stressor	Expected impact on GDL	Possible In-situ Test	Operating conditions
High electrode potential	Carbon corrosion	OCV or low current	$I_{cell} = 0 \text{ A cm}^{-2}$
Mechanical stress	Cracks / fiber damage	Temperature and humidity cycling	Cycling of T_{cell} between 60 - 95°C and RH between 120% - 30%; $I_{cell} = 1 \text{ A cm}^{-2}$
High temperature	Sintering and damaging of polymer, loss of hydrophobicity	Minimum cooling, heating	$I_{cell} = 1 \text{ A cm}^{-2}$, $T_{cell} = 95^\circ\text{C}$,
Particle erosion	Loss of carbon/polymer	High current density (high water production)	High current yielding e.g. 300 mV RH=100%/100%, high gas flow

High electrode potential. The results of the high electrode potential as possible operando stressor for the GDL are presented in this section. Apparently, the AST leads to severe voltage drop in the entire current density range as shown in Figure 21. The top panel depicts the polarization curves and the bottom panel shows the voltage recovery due to replacing the CCM and subsequently the GDL⁶. By replacing the aged CCM by a new one (EoT_CCM) the voltage losses are largely recovered except the current density range above 1.5 A cm^{-2} . Subsequent replacement of the aged GDL by a new one (EoT_Cathode GDL) does lead to a recovery of $<50 \text{ mV}$, which is relatively low and clearly shows that most voltage losses are associated to the CCM degradation, and most likely to the cathode catalyst layer and the membrane. The decrease of performance at EoT is linked to H_2 cross-over; Moreover, after EoT characterization an unexpected membrane failure occurred. Upon disassembly, the MPL was attached to the CL, which may affect the results shown in Figure 21. Even though the results have certain uncertainty, it seems obvious that the applied stressor has only minor effect on the cathode side GDL.

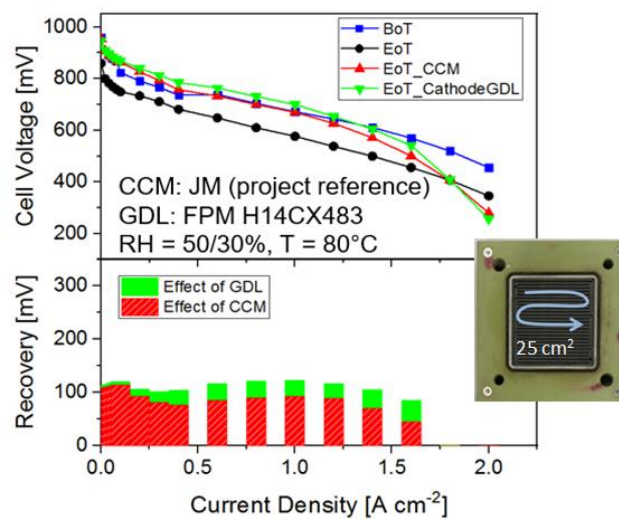


Figure 21: Analysis of high potential (OCV) condition as stressor using JM CCM and FPM GDL. During the test the cell was kept at OCV for $\sim 320 \text{ h}$ at 80°C , $100\% \text{ RH}$ and $250/230 \text{ kPa}$ (abs.) anode/cathode outlet pressure.

Mechanical stress. The cell was operated at 1 A cm^{-2} at 80°C with the stoichiometry of 1.5 for both H_2 and air. To induce stress the cell temperature was continuously cycled between 60°C and 95°C while keeping the absolute water content in the feed gases constant, leading to cycling of the RH between 120% and 30% . The tests were composed of around 150 cycles. One test was carried out using JM CCM and Freudenberg GDL H14CX483, and the other one using Gore CCM along with Freudenberg GDL H14CX483. The results of both tests are provided in Figure 22. The top panels depict the polarization curves, subsequently the voltage recovery due to replacing the CCM as well as the GDL, and the bottom panels depict EIS spectra.

⁶ Note, this is a deviation from the scheme in Figure 0.

Clearly, at EoT substantial losses are observed especially in the mass transport region of the polarization curve. When replacing the aged CCM with a new one, almost all the losses are recovered indicating that the stressor mainly affects the CCM. This observation is also confirmed by EIS measurements shown in the bottom part of the figures. At a current density of 1.2 A cm^{-2} the degradation rate over time assigned to the CCM corresponds to $\sim 1 \text{ mVh}^{-1}$ whereas the degradation rate due to the GDL is $< 0.1 \text{ mVh}^{-1}$.

Therefore, the mechanical stress as applied in this test is inefficient as operando stressor for the GDL. The loss of ECSA was calculated as 12% and 23% for the JM and the Gore CCM respectively along with slight thinning of the CCL, which was observed by SEM (data from WP2).

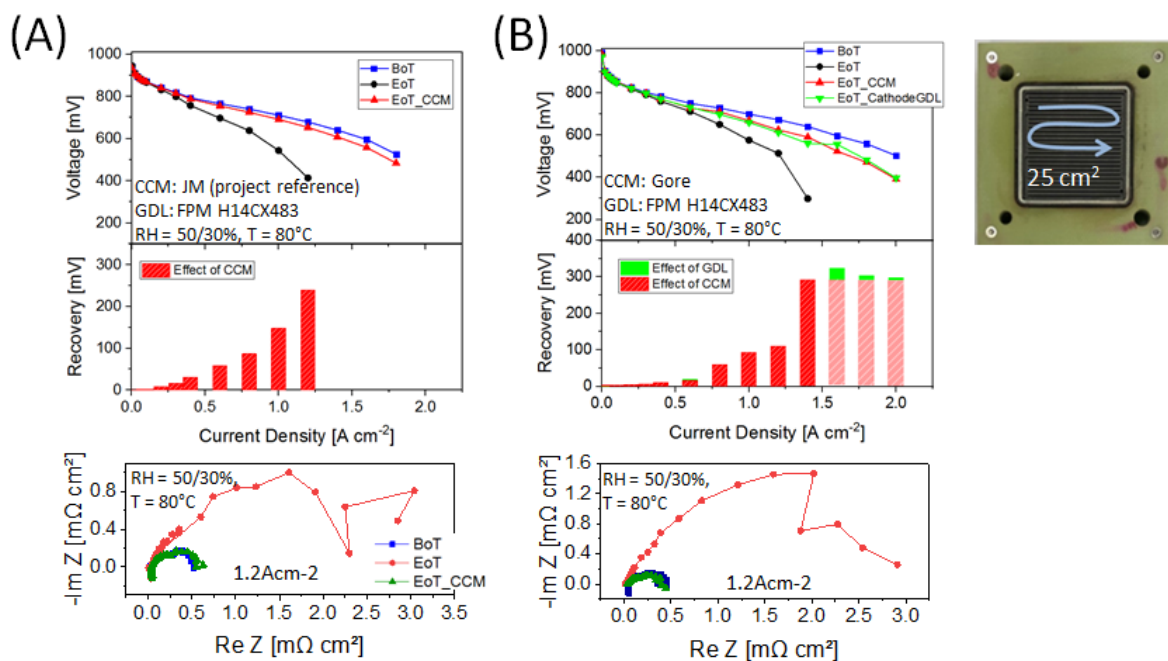


Figure 22: Analysis of mechanical stress on different MEA components. During the test, the cell was cycled ~ 150 times between 60°C and 95°C while keeping the absolute water content in the feed gases constant leading to cycling of the RH between 120% and 30%. During cycling the current density was kept at 1 A cm^{-2} , p (anode/cathode) was kept at 250/230 kPa(abs) and stoichiometries were 1.5/1.5 (anode/cathode). Performance curves and Voltage recovery evaluation during in-situ ASTs recorded at EoT, BoT, after exchanging the aged CCM by a new one (BoT_CCM) and after subsequently exchanging the aged cathode GDL by a new one (EoT_Cathode). The bright patterned boxes are assumed as lower limits for the CCM effects. (A) Test performed using JM CCM with FPM GDL. (B) Test performed using Gore CCM with FPM GDL. The flow field of the used cell is shown as an inset image.

High temperature as stressor. The cell was operated for 245 h at 1 A cm^{-2} at increased cell temperature of 95°C , 50% RH and stoichiometry of 1.5 for both H_2 as well as air. The test was performed using Gore CCM and Freudenberg GDL H14CX483. The corresponding polarization curves are plotted in Figure 23 (A). In panel (B) the overall voltage loss is plotted in comparison to voltage

losses assigned to CCM and GDL separately. Interestingly, the sum of losses measured using aged GDL and losses measured using aged CCM in Figure 23 (B) is much lower than the overall losses measured at EoT (without separating aged CCM and aged GDL). This effect, however, is observed when the polarization curves are recorder at nominal flow (corresponding to H₂ and air stichometry of 1.5/.1.5), but not at constant high gas flow (not shown). To rule out that the effect is due to disassembly/assembly of the cell, a specific test was carried out, the result of which is shown in Figure 23 (C) and described in the caption. The differences between polarization curves involving a simple disassembly/assembly of the cell without exchanging MEA components are significantly less than those observed in panel (A). Hence, the discrepancy between losses ascribed to the overall MEA, and the individual losses ascribed to the CCM and the GDL could be a coupling effect, *i.e.* combination of aged components have greater effect than the individual components replaced separately. Another possibility could be an insufficient refresh to eliminate reversible effects before EoT characterization.

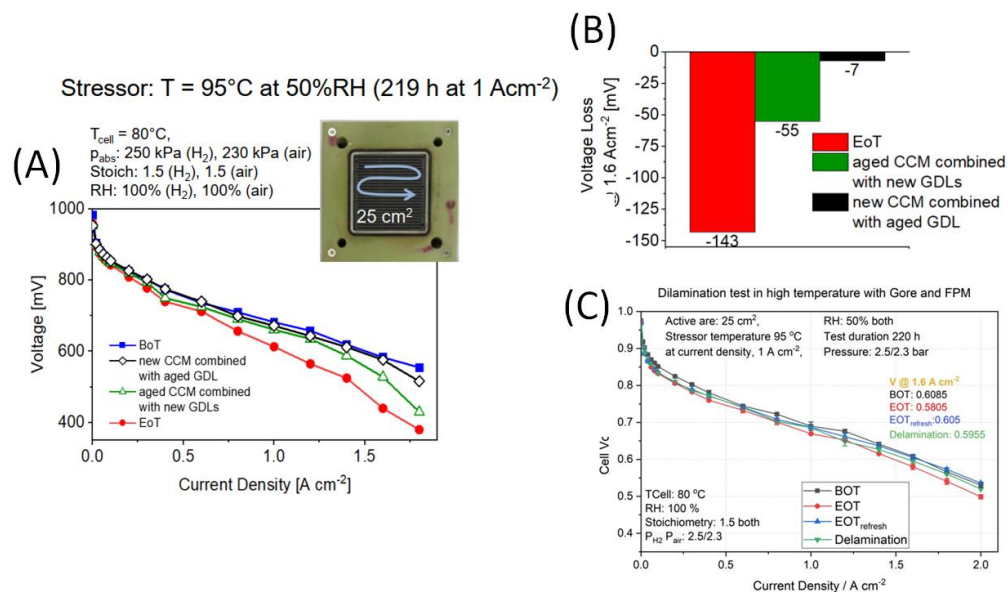


Figure 23: Analysis of high temperature condition as stressor using JM CCM and FPM GDL. The cell was operated for 219 h at 95°C, RH= 100 %, 250/230 kPa absolute anode/cathode outlet pressure and $\lambda_{anode} = 1.5$ and $\lambda_{cathode} = 1.5$.⁷ (A) Polarization curves measured at BoT, EoT and after combining aged CCM and GDL with new components. (B) Voltage losses measured at EOT and voltage losses due to CCM and GDL measured separately. (C) Polarization curves of a separate test; after 220 h at the above-mentioned conditions the cell was disassembled and assembled without exchanging the MEA components to determine the effect of disassembly/assembly.

Nevertheless, the key contribution to the performance loss can be attributed to the CCM degradation rather than to the GDL. Specifically, the CCL exhibits an ECSA loss of ~30% as well as slight thinning. To elucidate the effect of GDL in more detail ex-situ studies in WP2 are ongoing.

⁷ Results presented at 236th ECS Meeting in Atlanta.

Particle erosion. The cell was operated for ~ 290 h at $i = 4 \text{ A cm}^{-2}$, $T = 80 \text{ }^\circ\text{C}$, $\text{RH} = 100 \%$ and $\lambda_{\text{Anode}} = 8$, $\lambda_{\text{Cathode}} = 10$ yielding high water production due to high current density. To allow high gas flow the zero gradient test hardware was used. The test was carried out using JM CCM along with FPM GDL and Gore CC along with SGL GDL. Both tests lead to similar result. The corresponding polarization curves of the test with JM CCM and FPM GDL are depicted in Figure 24. When aged GDL is combined with a new CCM, virtually all voltage losses are recovered; the same effect can be concluded from the EIS spectra. On the other hand, when the aged CCM is combined with a new GDL, no performance recovery can be detected. Hence, the effect of CCM degradation is apparent and linked with 10-20% ECSA loss and light CCL thinning. Another effect is the inhomogeneous attachment of MPL with the CCL after MEA disassembly, resulting strong MPL delamination in the gas outlet region of cathode side.

Stressor: High water flux (300h, 100%RH, $j = 4 \text{ A cm}^{-2}$)

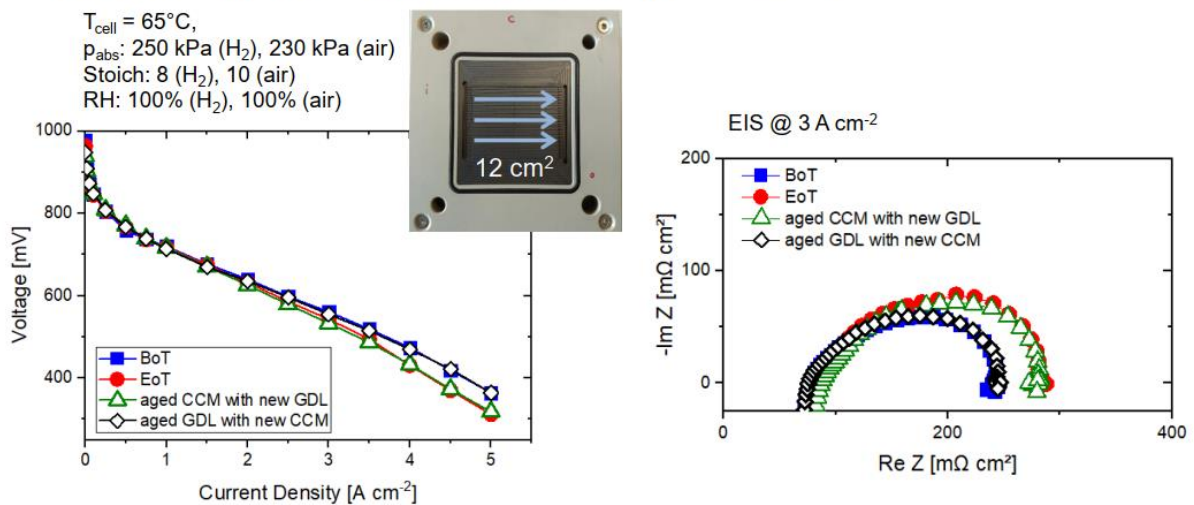


Figure 24: Analysis of particle erosion test using JM CCM and FPM GDL with a zero gradient test hardware.⁸ As stressor a current density of 4 A cm^{-2} at $\text{RH} = 100 \%$, 80°C , $250/230 \text{ kPa}$ absolute anode/cathode outlet pressure and $\lambda_{\text{anode}} = 8$ and $\lambda_{\text{cathode}} = 10$ was applied for 287 h. The condition for polarization curve acquisition is provided in the figure.

To further investigate the high water flux this stressor was combined with high temperature. A corresponding test was carried out by keeping the cell for 290 h at $i = 4 \text{ A cm}^{-2}$, $T = 95 \text{ }^\circ\text{C}$, $\text{RH} = 100 \%$ and $\lambda_{\text{Anode}} = 8$, $\lambda_{\text{Cathode}} = 10$. The degradation of the CCM was further enhanced in comparison to the high water flux test without elevated temperature leading to 35% ECSA loss at the CCL and Pt particle detachment. Moreover, after opening the cell for ex-situ analyses a pin hole in the CCM was detected.

⁸ Results presented at 236th ECS Meeting in Atlanta.



Summary. The effect of different stressors on the performance loss was analysed and leads to following preliminary summary.

- None of the ASTs selectively degrade GDL significantly, in all cases CCM degradation dominates. This is likely due to the high stability of the tested GDLs.
- At prolonged OCV condition membrane is the lifetime limiting component
- Mechanical AST: Temperature (60 to 95 °C) and RH cycling (30-120%) 150 cycles induces the highest overall voltage degradation in our study.
- Particle erosion (high water flux) seems to be a good AST candidate for the CL, since no effect on GDL is observed.

The overall degradation rates of the stressors cannot be easily compared because some can be expressed as voltage loss over time, but other, such as mechanical stress, cannot only be reported as voltage loss per event. Highest voltage loss over time was measured in case of the high temperature stressor with values around 1 mV/h at 1.5 Acm⁻². For the RH cycling test the decay rate is around 1 mV/cycle at 1.2 A cm⁻². For comparison, in another study⁹, a mechanical stress including freeze-thaw cycling was applied leading to a rapid decay of ~1 mV/cycle at 1.2 Acm⁻² during the first 30 cycles which dramatically slows down afterwards. The data from the provided test will be compared with the results from ID-Fast load cycling test to assess the acceleration factor of the stressors.

⁹ <https://linkinghub.elsevier.com/retrieve/pii/S0306261919300364>



6. Extended analyses of start-up/shut-down

Specifically, on/off periods may occur with a certain frequency that depends on the vehicle utilization and the energy management strategy implemented, but from a durability point of view a distinction is to be made between short stops and a complete system shut-down over a long time. In this last case, the ambient air is supposed to leak into the stack, specifically in the anode compartment, leading to the onset of a hydrogen/air front. A similar front develops when the system is started again, and the fuel injected from the tank displaces the leaked air. Start-up and shut-down events are recognized as a potential and critical issues for the fuel cells longevity.

Polimi adopted a reference start-up case following the specifications of the ID-FAST project durability test program. It is studied in the details of its dynamics by measuring the local currents and the local potentials that drive the degradation. A detailed local analysis of start-up events under different operating conditions is then performed. A systematic approach is followed to investigate the major stressors, *e.g.* temperature, residence time, oxygen partial pressure as depicted in Table 6.

Table 6 - Description of the stressor operating conditions on the start-up operation.

Stressor	Operating conditions
Mitigated start-up protocol	$T_{\text{cell}} = 30 \text{ }^{\circ}\text{C}$, $N_{\text{H}_2, \text{dry}} = 0.175 \text{ NI min}^{-1}$, RH 100%
H ₂ flow rate	$N_{\text{H}_2, \text{dry}} = 0.087.5/0.175/0.350 \text{ NI min}^{-1}$
Oxygen dilution at the anode compartment	Nitrogen, 5% O ₂ and air.
Cell operating temperature	$T_{\text{cell}} = 30/80 \text{ }^{\circ}\text{C}$
Shut-down	$T_{\text{cell}} = 30 \text{ }^{\circ}\text{C}$, $N_{\text{air, dry}} = 0.175 \text{ NI min}^{-1}$, RH 100%

Experimentally, an array of through-plate Reference Hydrogen Electrodes (RHE's) was implemented, to provide a spatially resolved in-operando measurement of each electrode potential with an extremely high temporal resolution. By the way of this technique, only limited attempts to measure the in-situ potential for this process can be found in literature, mostly focusing on the cathode side. RHE's were introduced in this work both at the cathode and at the anode to track the evolution of the local voltage profile. This information is combined with an innovative methodology for the measurement of the in-plane current generated during start-up/shut-down in a four macro-segmented hardware as described in Figure 25.

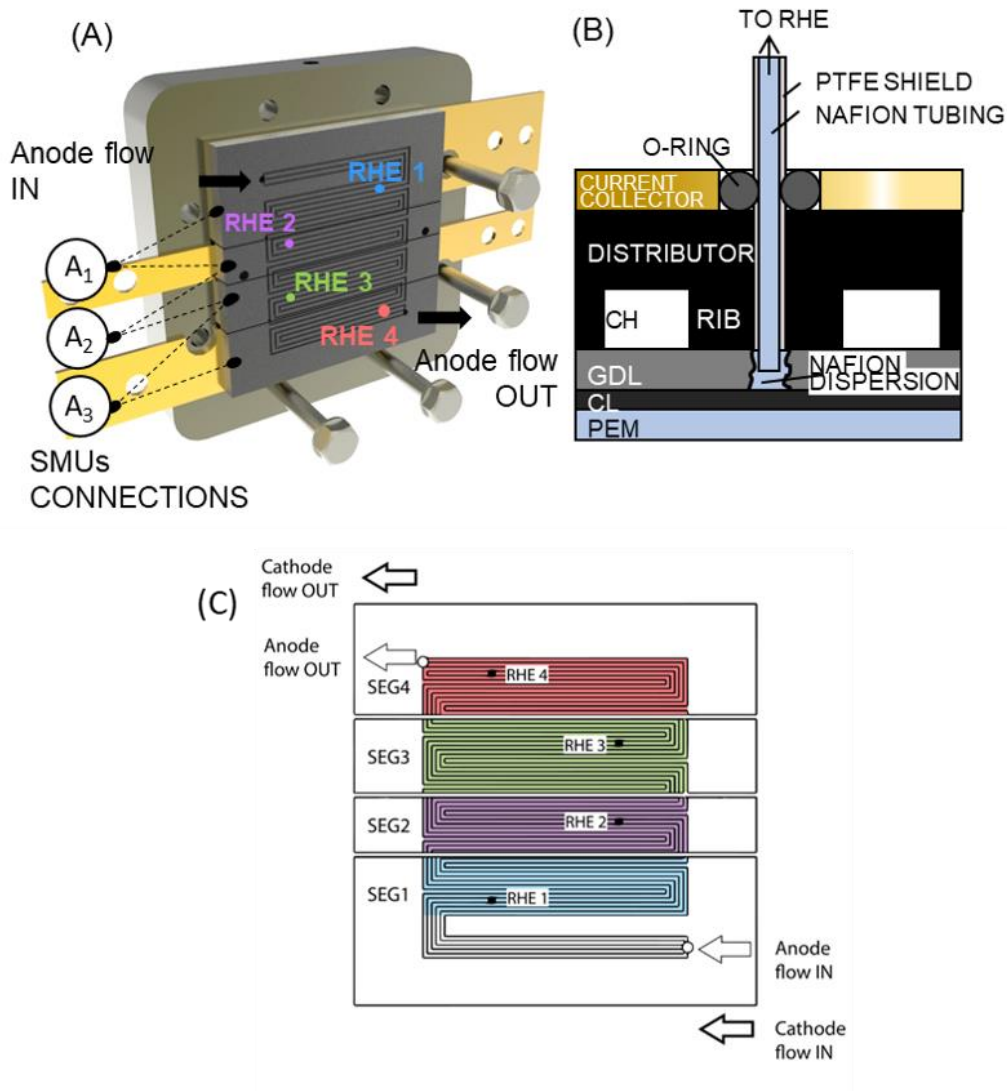


Figure 25 - (A) macro-segmented Fuel Cell setup with local potential electrode probe and in-plane measurement configuration. (B) Sketch of RHEs connection. (C) Geometry of the flow field where the division in segments and RHE's positions are evidenced.

During a start-up, the fuel-filled part operates regularly as a power supply (“active region”) and polarizes the oxidant-filled part (“passive region”) that operates as an electrolysis cell. In the following, the terms anode and cathode will be improperly used to indicate the two sides of the cell referring to normal active operation, independently of the reactions occurring. As a result of this heterogeneous situation, an internal current compensates the simultaneous generation and consumption of charge occurring at different positions along the same electrode, in dependence on the hydrogen/air front location. In other words, the reverse proton flow in the air/air and in the hydrogen/air regions leads to a circular current flow in the cell. Figure 26(A) show the local electrode potential measured in the positions highlighted in Figure 25(C), while in Figure 26 (B) the local in-plane currents drawn in each segment are plotted for experiment. As hydrogen is supplied, the HOR taking place makes the first segment an active region having a negative current. The other segments (2, 3, 4) behave as passive

regions, until hydrogen arrives in their sections: this occurs when their associated current evolves from positive to negative. Coherently to the current measurements, local RHE's show an increase in the cathodic potential when the MEA portion behaves passively: the 4th RHE reaches potentials as high as 1.6 V. Then, potential values fall to those typical for PEMFC operations when the MEA region switches to an active functioning. The anode potential moves instead from the open circuit potential when exposed to air flow (≈ 1.05 V), to the hydrogen equilibrium potential (0 V). The open circuit potential under air is found to be different from theoretical equilibrium value expected for ORR in the experiment, and this effect is attributed to the presence of Pt surface oxidation parasitic reactions. Figure 26(A) show also how the potential evolves at the anode side (dashed lines),

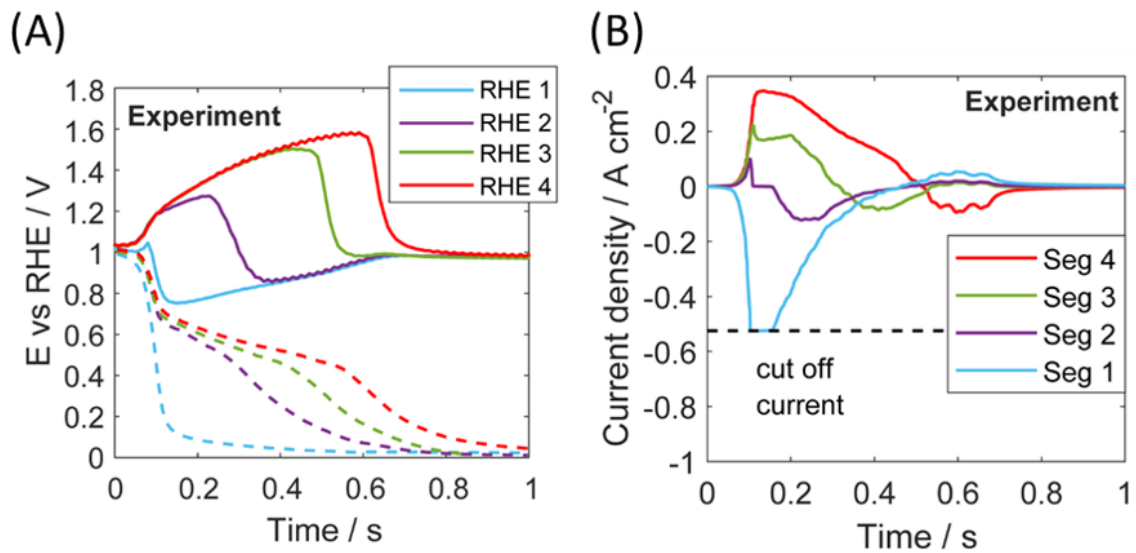


Figure 26 – Reference start-up, $T = 30^{\circ}\text{C}$, $\text{RH} = 100\%$, and anode dry flow equal to $0.175 \text{ NI min}^{-1}$ (residence time of 0.5 s). (A) Local cathode (solid line) electrode potentials and local anode (dashed lines) electrode potentials. (B) total currents drawn by each segment.

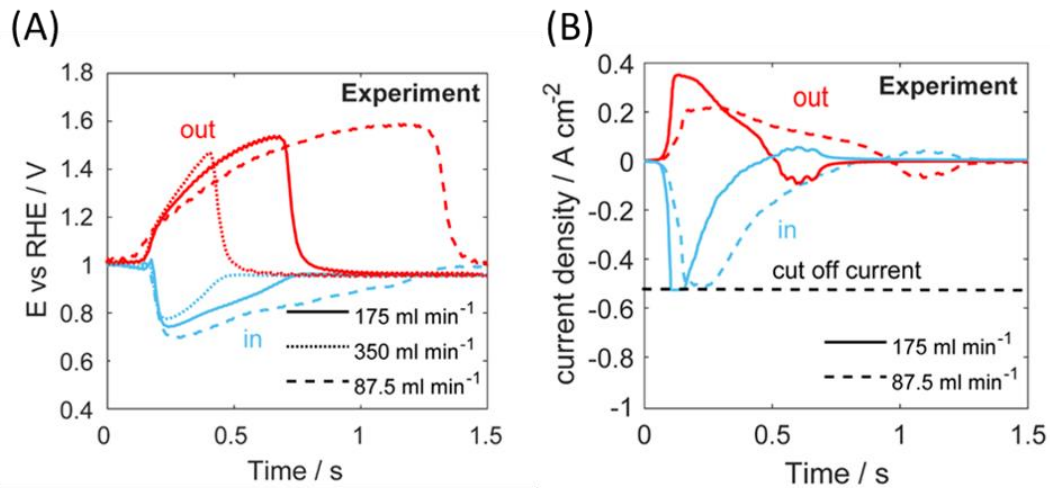


Figure 27 - Impact of the H_2 flow rate during start-up. (A) local cathode electrode potentials in case of 0.087, 0.175 (reference case) and 0.350 $NI\ min^{-1}$. (B) currents density drawn by each segment in case of 0.087 and 0.175 $NI\ min^{-1}$. In red, RHE_4 and segment 4 (out). In blue, RHE_1 and segment 1 (in).

In literature, start-up duration is commonly described through the residence time. According to a plug-flow model, a complete gas replacement is assumed at the anode side: the residence time corresponds to the time necessary to the in-flow to completely fill the available volume. For the reference start-up case, the residence time results equal to 0.5 s, which corresponds to a flow velocity of $1.25\ m\ s^{-1}$. Actual process duration was estimated instead from the experimental data: from the local voltages, when all the RHE's reach a homogenous air potential, and from the in-plane currents, as all the segments show simultaneously a null value. The experimental profiles, reported in Figure 27, of the local potentials and of the internal currents highlight a reference process duration of about 0.67 s ($\approx 35\%$ longer than theoretical). In this work, we observed that the plug-flow assumption underestimates the transient duration. Different dry flows have been tested while keeping constant the relative humidity and the temperature, as depicted in Figure 28. At $30\ ^\circ C$ and 100% RH, the dry anode flows imposed are: $87.5\ ml\ min^{-1}$, $175\ ml\ min^{-1}$, $350\ ml\ min^{-1}$. They correspond respectively to a residence time of 1 s, 0.5 s and 0.25 s. The increase of the flow rate and, hence, the reduction of the residence time, impacts on the potential profile: not only the lasting of the phenomenon (and so of the high voltages) is reduced, but also a lower maximum potential is reached (e.g. 1.5 V for $350\ ml\ min^{-1}$). On the other hand, larger internal currents are measured: the capacitive contributions increase because of a more rapid variation of the voltage profile. This is the result of the larger current peaks, even if the lasting of the transient is reduced, as visible comparing the full lines and the dashed lines in Figure 27(B).

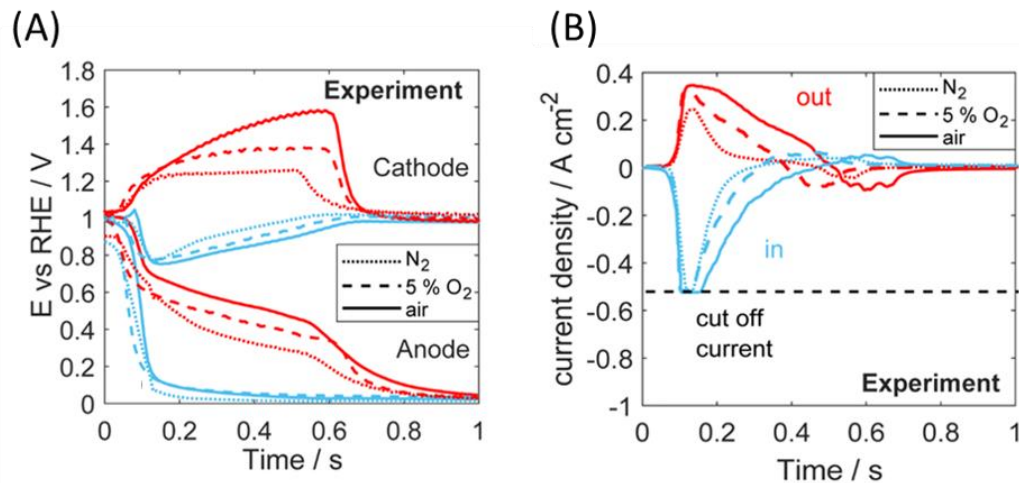


Figure 28 - Effect of the oxygen dilution at the anode compartment during start-up in case of N₂, 5% O₂ and air. (A) anodic and cathodic electrode potentials. (B) in-plane current densities. In red, RHE4 and segment 4 (out). In blue, RHE1 and segment 1 (in).

Data were also obtained in case of several oxygen concentrations present in the anode channel, GDL and catalyst layer before the start-up. Results are collected in Figure 28. Oxygen concentration is a parameter of interest since air leakages that occur during the long stop time could result in different gas compositions. A lower oxygen concentration influences the polarization behaviour of the negative electrode since it has a great impact on ORR: the anodic plateau-region in the air/air section of the MEA shifts towards a lower equilibrium potential. The voltage reduction at the anode helps in reducing the driving force for the reverse-current mechanism and the cathodic potential of the “passive” region drops down too; a minimum of 1.25 V is found for the nitrogen case (dotted line). As the oxygen concentration is decreased, also the internal currents are visibly mitigated, as collected by the experiments of Figure 28(B). Furthermore, the results obtained at very low oxygen concentrations, and most of all in the nitrogen case, revealed the impact the capacitive phenomena. Non-negligible currents are measured: when the anodic ORR in the passive zone is switched off, the reverse-current is fed by the anodic double-layer and by the PtOx reactions. Indeed, even in presence of an inert atmosphere, the anode electrode moves from a potential close to the air equilibrium value because of the oxygen crossover, that makes the anodic Pt surface oxidized. At low oxygen partial pressures, there is less amount of oxidant to remove. The process results to be faster since, even if the replacement is markedly plug-flow controlled, also the oxygen consumption plays a role, thanks to ORR and the direct reaction with the fuel.

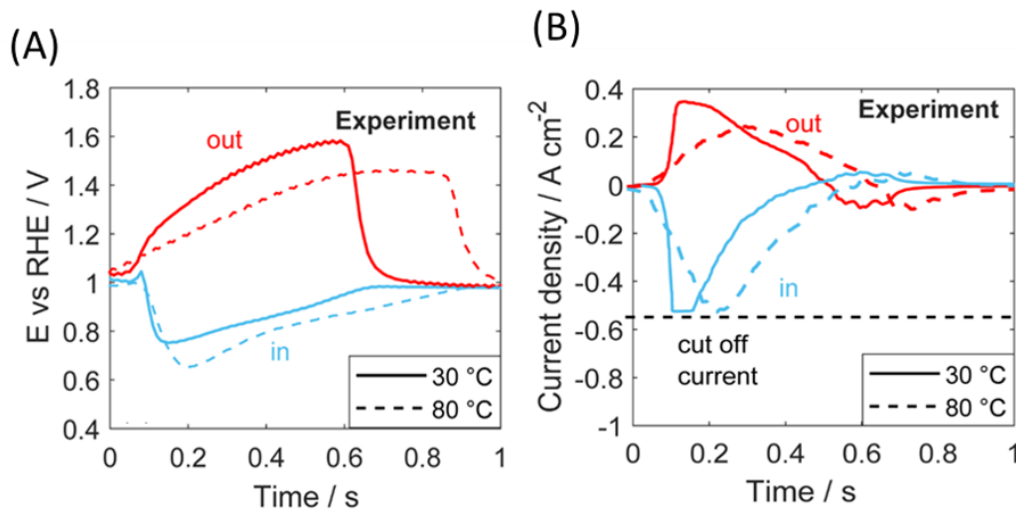


Figure 29 - Effect of cell operating temperature during start-up. (A) local cathodic potentials and (B) current densities. In red, RHE4 and segment 4 (out). In blue, RHE1 and segment 1 (in).

The 30 °C case was chosen as reference condition to mitigate the H₂/air front as occur in ID-FAST test plan, but higher temperature values (40 °C, 60 °C, 80 °C) were tested to evidence this mitigating impact of the ambient temperature operation. Firstly, results evidence higher cathode potential peaks and higher in-plane currents at ambient temperature. In particular, the maximum voltage decreases to 1.45/1.5 V at 80 °C. Secondly, the transient at high temperature lasts more than at low temperature: this should be caused by the lower partial pressure of hydrogen, since the higher partial pressure of water, that slows down the progress of the front because of gas diffusion and consumption. RHE1 gives a good indication for the active region of the cell: the minimum potential reached by the cathode is lower at high temperature. In other words, the overpotential for ORR.

These considerations on the stressors effect of the operating conditions will be used for the study of start-up / shut-down protocols and the development of a new AST representative of the process.

7. Development of a new AST related to start-up

Start-up/shut-down protocols

To reproduce start-up/shut-down cycle both with and without mitigations, two protocols have been appositely developed at Polimi, to investigate degradation associated with such operation. These protocols are named “un-mitigated start-up/shut-down” and “mitigated start-up/shut-down” and described in Table 7 and Table 8 - Mitigated start-up/shut-down protocol at 30 °C, 100% RH, ambient pressure. Un-mitigated SU/SD operation is summarized in Table 7.



Table 7 - Un-mitigated start-up/shut-down protocol at 80°C, 100%RH and ambient pressure.

Step	Name	Description
#1	Refresh	300 s (since cathode potential decreases below 100 mV): H ₂ /cathode closed
#2	Standby	60 s: OCV in H ₂ /Air
#3	Start-up (SU)	Allow hydrogen flow at anode and wait 60s
#4	Shut-down (SD)	Allow air flow at anode and wait 60s
#3 - #4 repeated 5 times in a row		

The protocol started with a refresh procedure (#1), applied to prevent any influence of the eventual catalyst surface oxidation: the flux at cathode is interrupted and the voltage is let decrease thanks to H₂ crossover from the anode, promoting cathode catalyst oxides reduction. After the cell voltage decreases to a value as low as 100 mV, a condition that is held for 5 min, a sequence of SU/SD cycles (#2-#4) is performed, as occur in consecutive cycle of SoA support AST. A H₂/air OCV condition (#2) is held for 60 s to simulate post-operation transient, then five in-a-row shut-down (#3) and start-up (#4) transients are performed, implemented as an air flow at anode followed by the H₂ flow. The protocol was performed at 80°C, with fully humidified gases both at anode and cathode side. The anode fluxes were set to $N_{H_2/Air} = 0.05 \text{ NI min}^{-1}$ and at the cathode $N_{Air} = 0.2 \text{ NI min}^{-1}$.

A full diagnostic protocol is periodically performed during start-up/shut-down protocol cycling. EoT (end-of-test) was chosen considering a minimum performance of 0.3 V during galvanostatic operation at 0.4 A cm⁻².

Consistently to the protocol described in WP1, a modified SU/SD protocol has been also developed to simulate the execution of H₂/air front in presence of mitigation strategies as in state-of-the-art automotive systems. The mitigated SU/SD protocol is described in Table 8.

Table 8 - Mitigated start-up/shut-down protocol at 30°C, 100% RH, ambient pressure.

Step	Name	Description
#1	Refresh	300 s (since cathode potential decreases below 100 mV): H ₂ /N ₂
#2	Mitigated shut-down (SD)	120 s: Air/N ₂
#3		120 s: Air/Air
#4	Real start-up (SU) or H ₂ /air front	120 s: OCV in Air/H ₂
Repeat #1 - #4 every 660 s		

Also, the mitigated protocol started with a refresh procedure (#1). N₂ is fluxed at cathode side for 300 s, during which cathode potential decreases till approximately 100 mV. After the purging of the oxidant by the inert, air is fluxed for 120 s through the anode (#2). Cell voltage immediately drops further, till 0 V. Same voltage is kept when air is introduced into the cathode (#3): the post-long stop

air/air condition is finally reached and high cathodic potentials are avoided during the shut-down transient which is thus defined as mitigated. After 120 s, a H₂/air front (#4) is finally generated at anode side causing the start-up.

After 120 s again, the described procedure is repeated. According to indications provided by car manufactures, the flux of hydrogen during start-up must be 1 A cm⁻² equivalent. Using a 25 cm² CCM, N_{H₂} = 0.175 NI min⁻¹; the same value has been adopted for the air flux at anode side. Applying this specification also to the cathode, it results N_{N₂} = N_{air} = 0.417 NI min⁻¹.

Degradation analysis under un-mitigated start-up/shut-down protocol

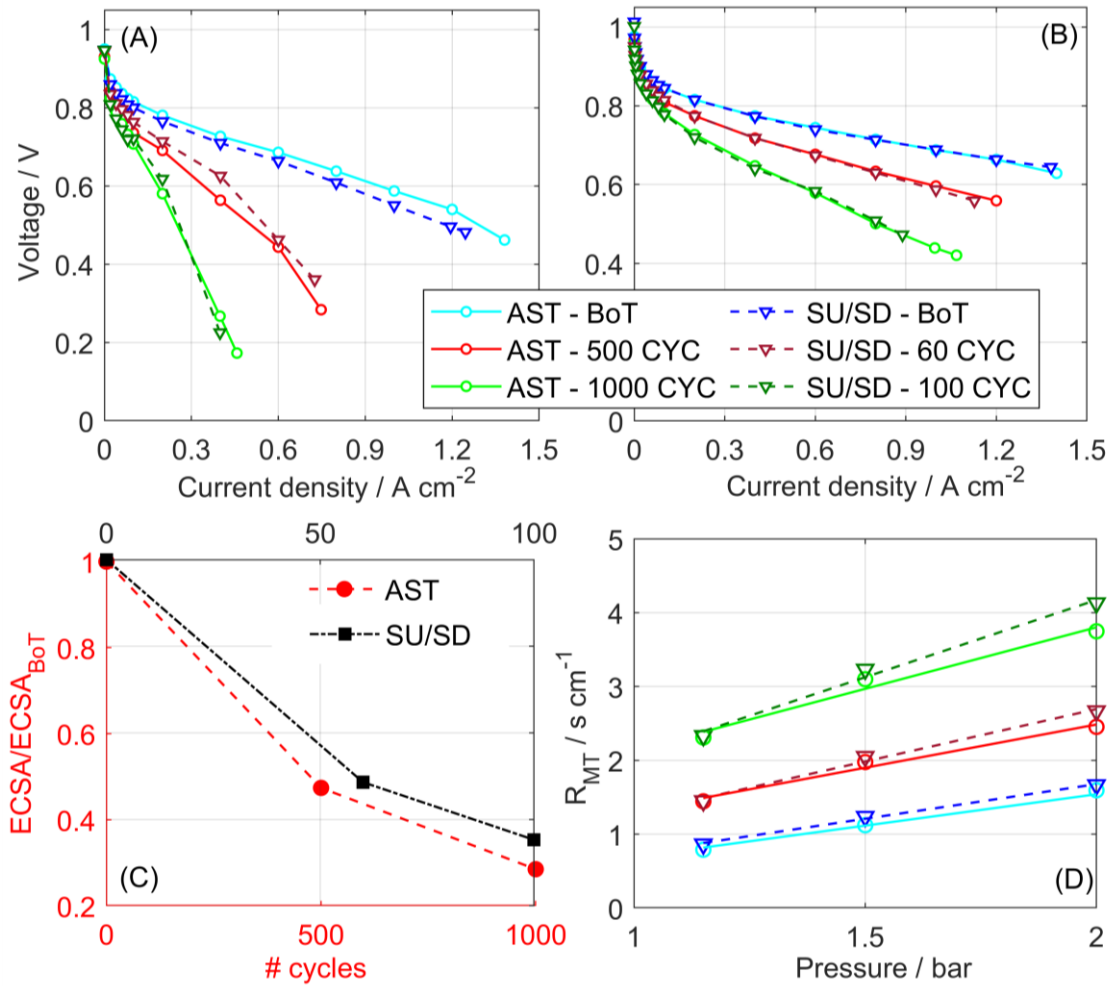


Figure 30 - Degradation analysis, on ION POWER MEA, after 1000 cycles of DoE catalyst support AST and 100 cycles of un-mitigated SU/SD in 25 cm² single-cell: (A) air and (B) pure oxygen polarization curves evaluated at: T = 80°C, RH=100%, P = ambient, stoich. An/Ca = 2/4, (C) Relative change in ECSA (normalized to the ECSA at BoT) vs. the number of cycles, conditions: T = 30°C, RH = 100%, P = ambient, and flow rates of 0.06 NI min⁻¹ for H₂/N₂ (anode/cathode), (D) oxygen mass transport resistance measured at P = 115/150/200 kPa_(abs) and three oxygen concentration (X_{O₂dry} = 1/2/3 %).



The aim of the work presented here is to clarify and quantify the degradation caused by abovementioned SU/SD operation, in absence of any mitigation strategy. The attention is primarily focused on catalyst layer support failure which is known to be the most relevant issue related to SU/SD. Hence, as first step of the work, the aging effect driven by 1000 cycles of the carbon support AST protocol are compared to those given by 100 cycles of start-up/shut-down processes Figure 30 compare air and pure oxygen polarization curves of aged MEAs. Characterization was performed at BoT, 500 and 1000 cycles of AST, while un-mitigated SU/SD operations was analyzed after 60 and 100 cycles.

Polarization curves at 60 and 100 SU/SD are respectively in good agreement - both in oxygen and air - with 500 and 1000 cycles of support AST, indicating a factor of 10 in terms of cycles, thus acceleration factor in time of 6 for AST (considering respectively the duration of the SU and SD operations of 60s each). This consistency of performance fading of support AST with SU/SD operation indicates that the main aging mechanism found in un-mitigated SU/SD is indeed corrosion of carbon support, in agreement with the literature findings. To confirm this, performance evolution was investigated by electrochemical measurements to clarify the different contributions expected to be caused by carbon corrosion mechanism.

The evolution of ECSA of support AST is consistent with that of SU/SD operation as visible in Figure 30(C), which is shown to be halved after 500/60 cycles of support AST and SU/SD protocol respectively, and further reduced below 40% at EoT. Mass activity at 1000/100 cycles of support AST and SU/SD protocol respectively, is only the 39% and the 30% of the initial value, confirming SU/SD operation to dramatically impact on cathode electrode. The variation of mass activity shows good consistency with ECSA loss and is larger in the initial part of the test (500/60 cycles of support AST and SU/SD protocol respectively), with a reduction of almost 50% from BoT. This suggests that the largest loss of available catalyst sites occurs in the first stage. Mass transport resistance is plotted as a function of pressure and is depicted in Figure 30(D), showing again strong consistency between SU/SD and support AST.

In conclusion, has been demonstrated that the SoA protocol for catalyst support degradation is representative of start-up/shut-down operation, without mitigation strategies (*i.e.* T = 80°C, 100%RH and low flow-rate).

Degradation analysis under mitigated start-up/shut-down protocol

To assess the impact on the degradation of the catalyst support at low temperature (30 °C), as proposed in the ID-FAST protocol for the H₂ / air front, the DoE catalyst support AST was repeated at 30 °C. The results were collected on JM MEA and Freudenberg GDL adopting Zero-P Fuel Cell.

The AST results collected at 80°C and 30°C are depicted in Figure 31. At 80 °C, the ECSA reduces by 17% between 1 and 1000 cycles and decreases by 41 % in the last 4000 cycles. To evaluate the performance loss induced by voltage cycling, iR-free differential curves were compared at BoT and EoT. The voltage loss was respectively: -83 mV at 1 A cm⁻². After 5000 cycles, the theoretical voltage loss is -15 mV according to Tafel kinetics. The experimental results are higher compared to the theoretical calculations, suggesting that also worsening of proton and oxygen transport are involved. Low temperature (30 °C) support AST presents different results in terms of degradation effects than

high temperature AST. The active area increases uniformly during AST. In the first 500 cycles ECSA can be considered constant and reach the maximum value after 1000 cycles, after 5000 cycles the ECSA value is still 14% higher than at the beginning of test. Hence, in terms of ECSA, a degradation effect is not identified, confirming the mitigation role of the temperature, which has a strong impact on carbon corrosion kinetics. In conclusion, catalyst support AST at 30°C was not effective to reproduce performance loss observed in for real test (reported in Figure 32), during mitigated protocol, and hence the development of a new protocol is required.

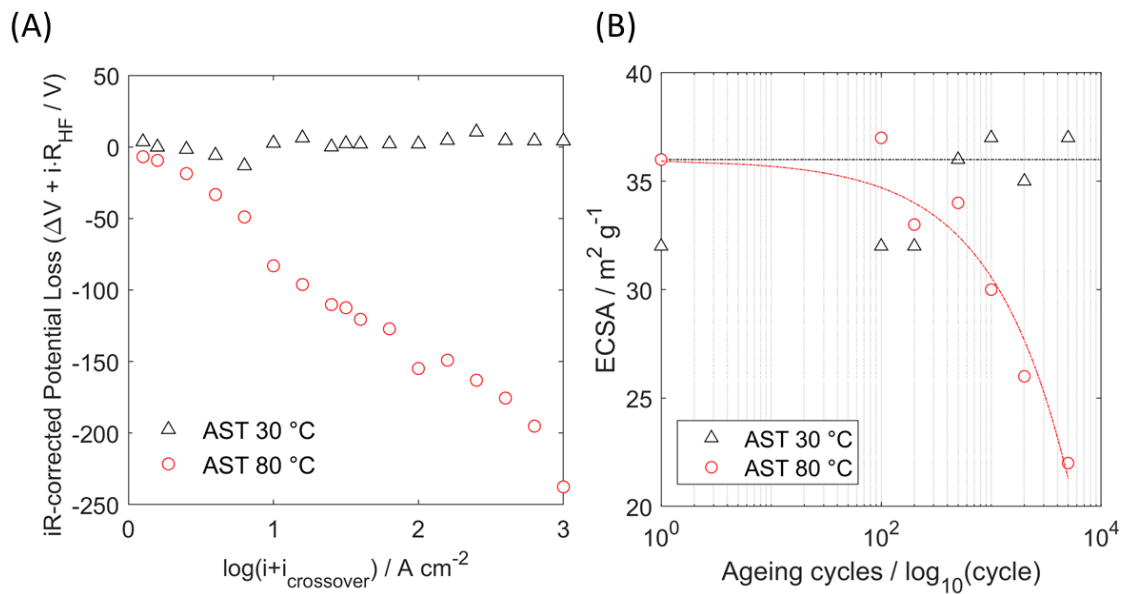


Figure 31 - Effect of temperature on support ASTs in Zero-Gradient cell on JMFC MEA: (A) Normalized voltage loss in reference condition: $T = 80 \text{ }^\circ\text{C}$, $RH = 100\%$, $p_{\text{anode}}/p_{\text{cathode}} = 250/230 \text{ kPa}$, stoich. $An/Ca = 8/10$, minimum flux = 0.5 A cm^{-2} equivalent. (B) ECSA during support ASTs.

In the following, the results of the ID-FAST H_2/air front operation on JM MEA and Freudenberg GDL are described. The 25 cm^2 macro-segmented Fuel Cell, as described in Figure 25(A), was adopted to test 200 cycles of mitigated start-up (H_2/air front) and shut-down operation as described in Table 8.

The mitigation of shut-down is expected to introduce strong heterogeneities, located at the cathode inlet/anode outlet region caused by the start-up performed in counter-flow configuration. To verify heterogeneous aging and identify specific differences respect to un-mitigated SU/SD operation discussed above, the performance loss of each MEA region is analysed and the results are reported in Figure 32.

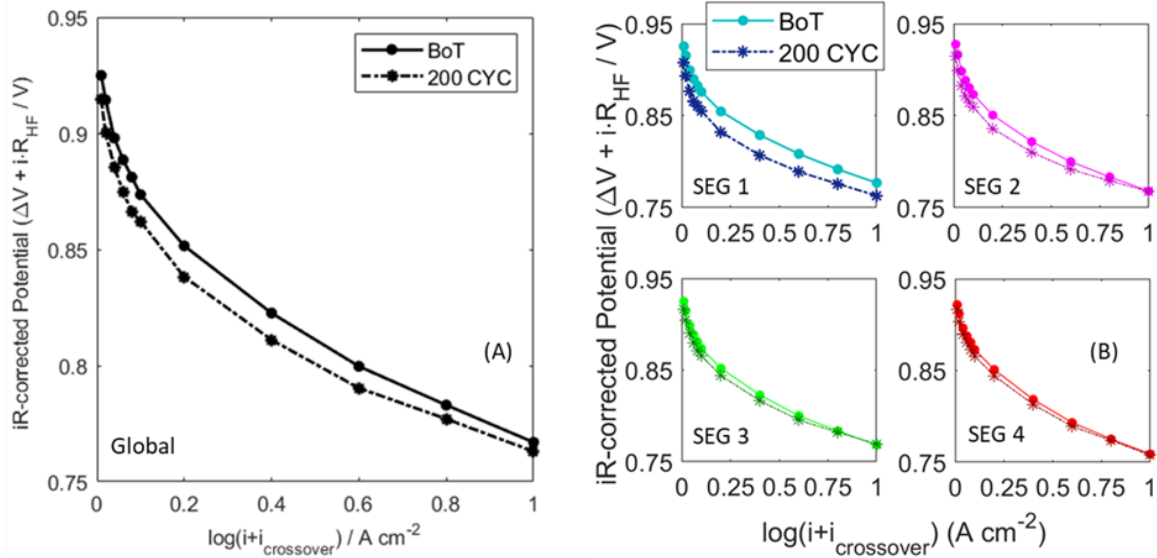


Figure 32 - Local aging analysis after 200 cycles of mitigated start-up protocol in segmented-cell on JMFC MEA: (A) Overall H_2 /Air polarization curve in condition: $T=80\ ^\circ C$, $RH =100\%$, $p_{an}/p_{ca}=250/230\ kPa_{(abs)}$, stoich. $An/Ca = 2/4$, (B) detailed of local polarization curves measured for each segment.

Polarization curve performed at BoT and EoT, are reported in Figure 32(A). A voltage loss of -12 mV at $0.4\ A\ cm^{-2}$ after 200 cycles was observed. Considering fading related to SU/SD in absence of any mitigation strategy discussed above (-480 mV loss at $0.4\ A\ cm^{-2}$ after 100 cycles), this confirms the sensible positive effect of the introduced mitigation strategy in limiting overall detrimental effects.

Interesting insights are obtainable by means of localized investigation: Figure 32(B) reports local polarization curves, focusing on low-current density range, which permits to detail the local degradation in the kinetic region. From their comparison, a sensible heterogeneity appears in terms of performance loss, noticeably stronger at cathode inlet region, in consistency with the high potential occurring during start-up transient. The performance loss, at $0.4\ A\ cm^{-2}$, for the four segments (moving from cathode inlet, SEG 1, to outlet region, SEG 4) are respectively: -22 mV, -13 mV and smaller for the third and fourth segment (-8 mV and -6 mV).

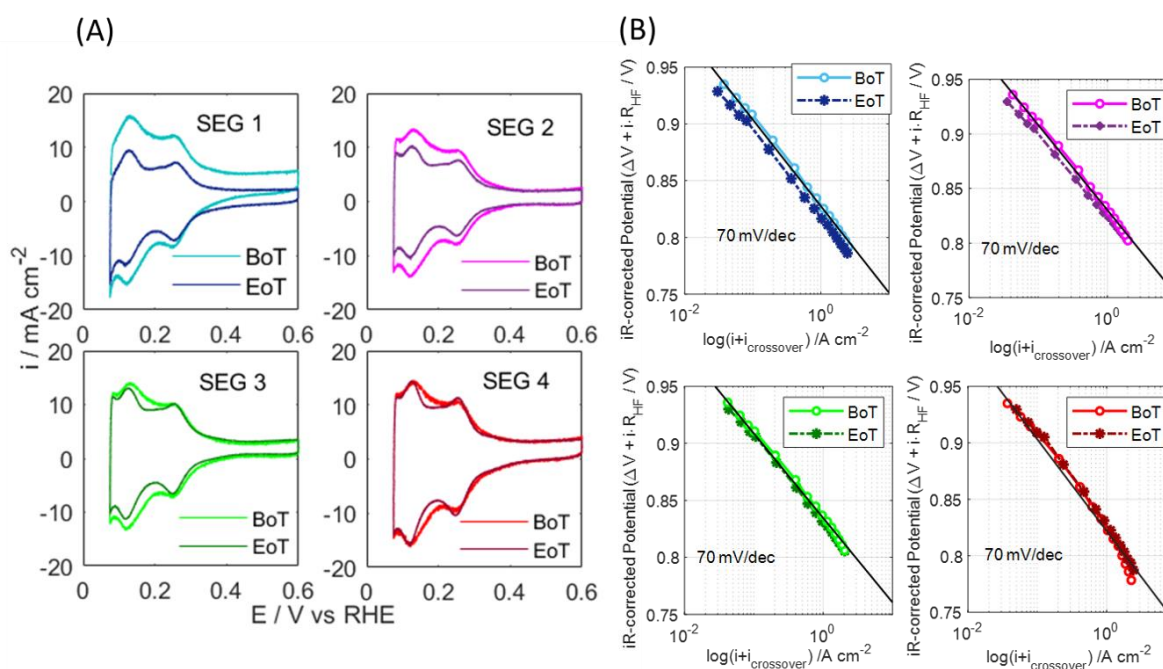


Figure 33 - Local CV of un-mitigated SU/SD at BoT and EoT. (B) Local O_2 polarization curves from cathode inlet (SEG 1) to cathode outlet (SEG 4).

Cyclic voltammetry, reported in Figure 33(A), confirms an uneven ECSA loss in the cathode catalyst layer. For an average ECSA loss of 25% with respect to BoT, local heterogeneity loss is evident beneath each segment. The largest loss is again localized at cathode inlet segment, confirming the harsher operation, and progressively milder towards the outlet section of the electrode.

H_2/O_2 polarization curves, reported in Figure 33(B), also demonstrate heterogeneous performance reduction, visible as a vertical translation in the i - V chart. The largest voltage decrease regards SEG 1 and 2 (close to anode outlet), respectively -11 mV and -11 mV (at 0.4 A cm⁻²), while the performance of the SEG 3 and 4 is respectively unchanged and even slightly improved (due to current redistribution between the segments).

For the first segment the so-calculated theoretical voltage loss curve is -14 mV, in good agreement with performance decay measured from H_2/O_2 polarization.

In conclusion, a large difference is found between the degradation in the un-mitigated and mitigated SU/SD. The difference was both quantitative (larger degradation is found for the un-mitigated case), and qualitative, because the voltage loss appears as an offset for any current density and localized in the air inlet region only. To get insight into these results, additional tests were performed in a zero-P Fuel Cell and a new AST protocol was defined to reproduce the degradation observed during mitigated start-up protocol.

New Start-up AST

A new AST protocol was developed (hereinafter defined Start-up Accelerated Stress Test, SU-AST) aiming to reproduce the local degradation identified at the air inlet in the mitigated start-up test performed in the segmented-cell hardware.

The definition of the SU-AST started from the analysis of the local cathode potential measured by RHE, focusing on the first segment, identified as the passive region during start-up, where the local degradation rate is higher.

Table 9 - Start-up protocols: AST steps and mimicked operation during real start-up cycle in macro-segmented Fuel Cell.

	Mitigated start-up in segmented cell	Start-up AST
Cycle	1) refresh H ₂ /N ₂ at OCV for 5 min (Stop with valve closed)	1) Potential hold at 0.1 V for 2.5 min
	Air infiltration in stack due to leakages	↓ Slow ramp at 0.1 V s ⁻¹ rate
	2) Air/N ₂ and Air/Air, long stop at ambient temperature	2) Potential hold at 1 V for 4 min
	Hydrogen/Air front at anode compartment	↓ Fast ramp at 1.5 V s ⁻¹ rate
	3) Start-up	3) Peak at 1.5 V
		↓ Fast ramp at 1.5 V s ⁻¹ rate
	H ₂ /Air operation	4) Potential hold at 1 V for 1 min
Cycle duration	660 s	
Temperature	30°C	
RH	Anode/Cathode 100%	
Pressure	Atmospheric	
Reactants	Anode/cathode – 0.175/0.417 NI min ⁻¹	H ₂ /N ₂ – 0.06/0.06 NI min ⁻¹

The mitigated start-up protocol is reported in Table 9. During the cycle, the potential profile at cathode inlet (*i.e.* SEG 1) and the cell voltage were collected and results are reported in Figure 34(B). After the refresh period under H₂/N₂, air was fed in the anode compartment. Potential increased at about 1 V vs RHE and remained almost constant until the end of the cycle with a fast voltage cycling at 1.5 V during H₂/air front.

The target of the new AST cycle is to reproduce the effects of the real potential profile in the same operating conditions. The new SU-AST proposed is consistently performed at low temperature (*i.e.* $T = 30\text{ }^{\circ}\text{C}$) and with the fuel cell fed by 0.06 NI min^{-1} of N_2 at the cathode and by 0.06 NI min^{-1} of H_2 at the anode.

To simplify the shape of the voltage profile in real start-up and increase reproducibility, a triangular sweep cycle is proposed. Cathode potential is symmetrically scanned at 1.5 V s^{-1} rate between 1.0 V and 1.5 V vs RHE. Voltage profile is reported in Figure 34(C).

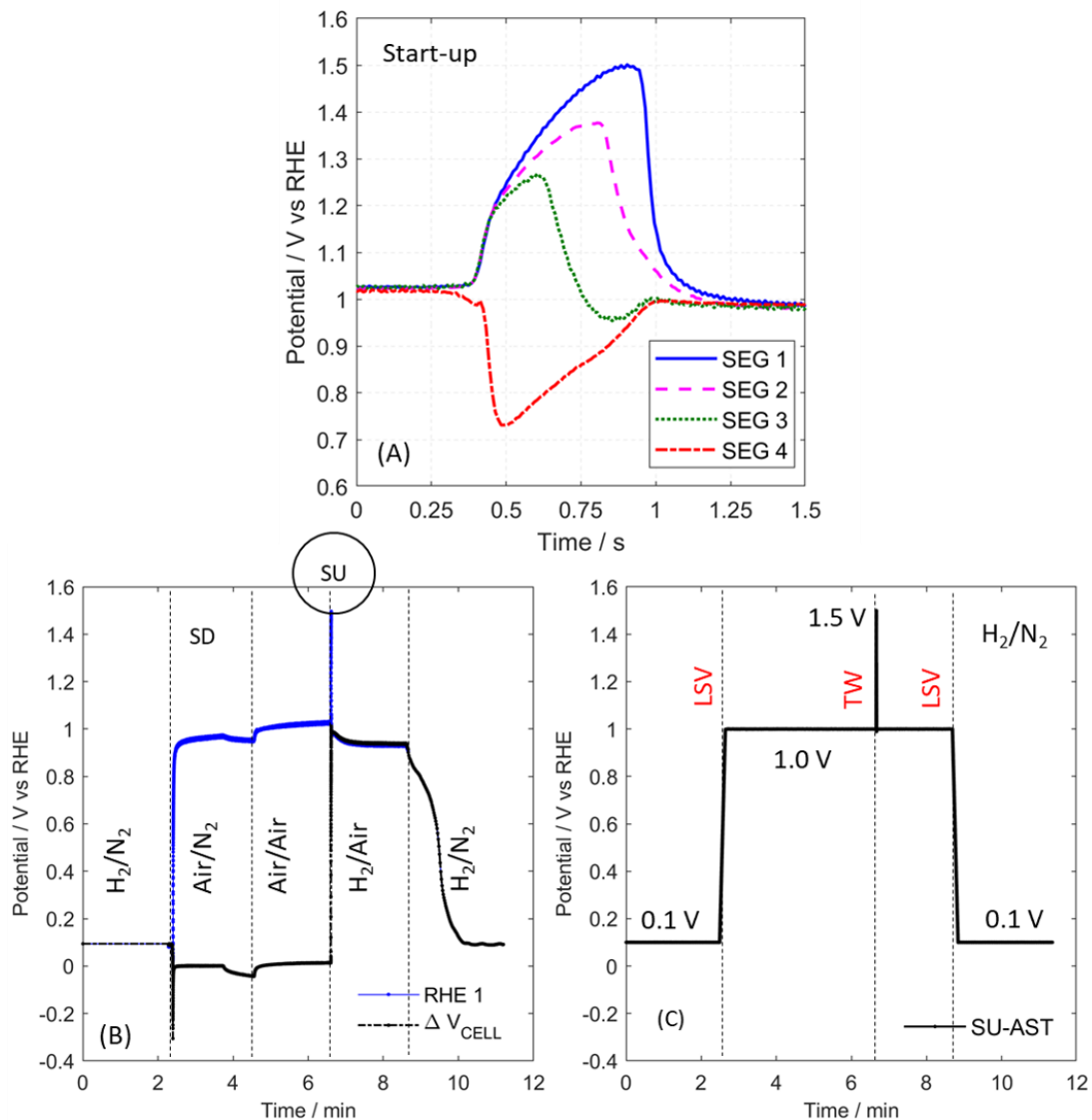


Figure 34 - Potential profile during start-up operations on JMFC. (A) Local potential profile collected with RHE at four-segment regions during H_2/air front (counter-flow configuration), (B) Comparison between local potential profile at cathode inlet position and cell voltage during one cycle of mitigated start-up in segmented-cell, (C) Potential profile adapted for start-up AST performed in zero-gradient cell.



To demonstrate the consistency of the SU-AST in terms of aging effects, 200 cycles were performed in Zero-P Fuel Cell and were compared to 200 mitigated SU/SD cycles operated in the segmented-cell hardware. To enable a direct comparison between tests on the two different hardware, iR-free polarization curves are plotted in Figure 35(A). For the scope, this correction makes acceptable the comparison between the two hardware, at least, up to 1 A cm^{-2} .

The results demonstrate a noticeably good reliability for the SU-AST in reproducing the effects of actual SU/SD operation localized at cathode inlet. The performance loss is respectively: -21 mV and -22 mV (at 0.4 A cm^{-2}) for the real SU at cathode inlet and SU-AST in zero-gradient cell, respectively.

In terms of ECSA loss, the degradation obtained at 200 cycles of the SU-AST is comparable with the one obtained in the first segment, as presented in Figure 35(B).

The oxygen mass transport resistance (R_T) was analysed and correlation with the inverse of roughness factor is reported in Figure 35(C), to elucidate the degradation mechanism. The results of real start-up and SU-AST are compared with DoE electrocatalyst protocol, and support protocol, both performed at 80°C , and finally with a combined protocol that consist of a sequence of electrocatalyst AST at 80°C and start-up AST. First, it is important to point out that the shape of the flow-fields in zero-gradient and segmented hardware are different, the land of segmented-cell flow-field is almost three times the land of zero-gradient cell flow-field. For this reason, limiting currents are lower in the segmented-cell leading to higher oxygen transport resistance (R_T).

The evolution of the R_T , in the case of the electrocatalyst AST was analysed. A linear correlation is found and slope of the straight line through the $r.f.^{-1}$ values, for each test pressure was found as: 10 s/cm at 150 kPa , 10 s/cm at 250 kPa and 7.5 s/cm at 350 kPa (for tests performed at 80°C and $\text{RH} = 100 \%$). Additionally, for the electrocatalyst AST, the computed value of R_{p1} fit a straight-line as a function of $r.f.^{-1}$, and the regression slope, $R_{O_2,Pt}$ is $= 12 \text{ s/cm}$, according to literature¹⁰.

The linear relationship observed for a Pt dissolution mechanism, is no longer valid for the support AST. Here, the evolution of R_T during AST is well-fitted with a quadratic function, in accordance with the degradation of electrode microstructure as foreseen by studies on carbon corrosion mechanism.

However, in the case of the mitigated start-up and in the case of the AST start-up, a linear trend was observed between the beginning and the end of life after 200 cycles, which is compatible with a degradation mechanism associated with platinum dissolution. To confirm the results, the evolution of R_T under combined test of electrocatalyst and start-up ASTs performed in row was analyzed. Here, the R_T values, at three different pressures, extend the linear trend observed of the electrocatalyst AST. These results highlighted the main role played by Pt dissolution mechanism during mitigated Start-up protocol proposed that is also confirmed by *post-mortem* analysis.

¹⁰ Greszler, T. a., Caulk, D., & Sinha, P. (2012). The Impact of Platinum Loading on Oxygen Transport Resistance. *Journal of The Electrochemical Society*, 159(12), F831–F840. <https://doi.org/10.1149/2.061212jes>

A general approach to identify transfer function from zero-gradient Fuel Cell to real-world operation on full-scale cell was here proposed. It is based on the achievement through the investigation of physics of the mechanisms of reverse-current during start-up and shutdown, and the analysis of local performance losses, under the specific protocol developed, introducing mitigation strategies to mimic real automotive stack start-up/shut-down operation.

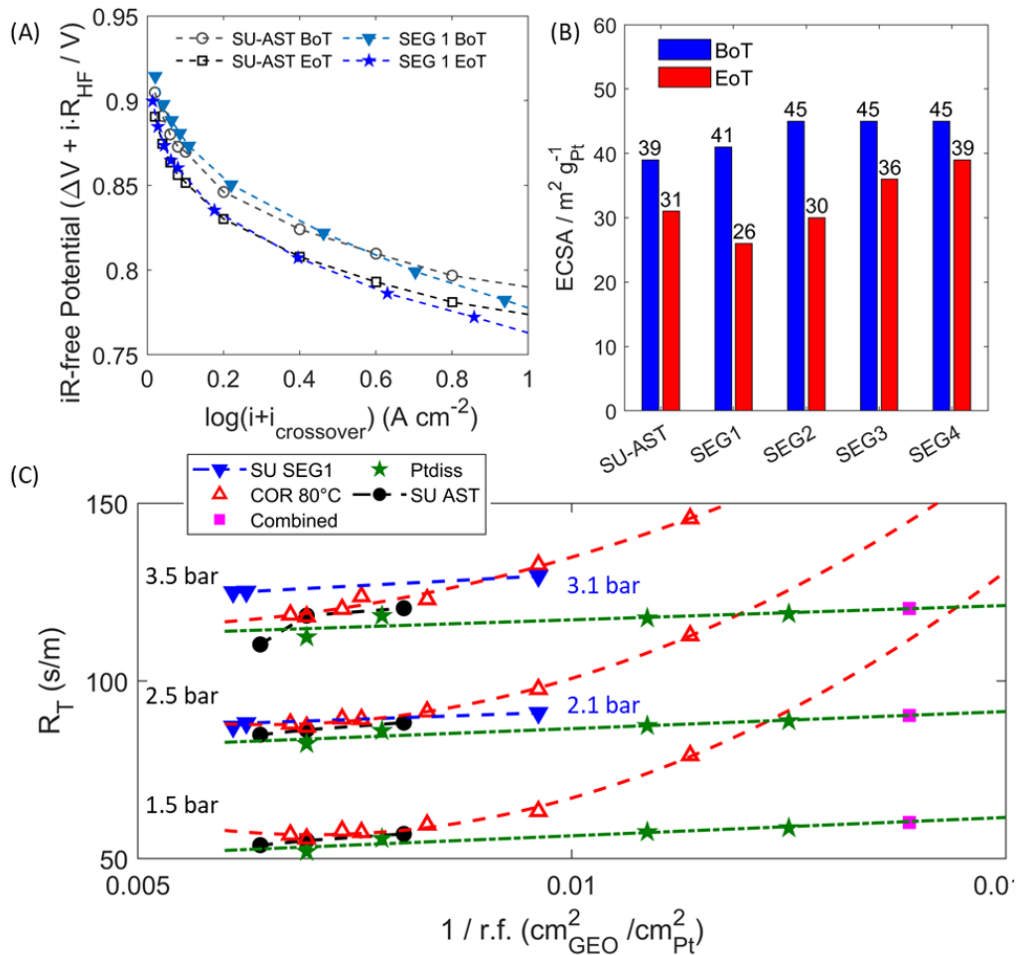


Figure 35 - Comparison between start-up AST and cathode inlet segment of mitigated start-up/shut-down after 200 cycles of operation on JMFC. (A) iR-free H_2 /Air polarization curves measured at $T = 80\ ^\circ C$, $RH = 100\%$, $p_{anode}/p_{cathode} = 250/230\ kPa$, the full symbols represent segment 1 of MEA in $25\ cm^2$ segmented-cell while the open symbols is the $10\ cm^2$ MEA in zero-gradient cell; (B) ECSA comparison for AST and mitigated SU/SD at each MEA segment; (C) Oxygen transport resistance plotted against the inverse roughness factor for 3 different pressures in zero-gradient cell ($P = 150/250/350\ kPa_{(abs)}$), and 2 pressures for segmented-cell ($P_{SU-SEG1} = 210/310\ kPa_{(abs)}$). For each point R_T was interpolated from 3 different oxygen concentrations ($X_{O_2dry} = 1/2/3\ \%$). The reported tests for zero-gradient cell are: electrocatalyst AST (Ptdiss), catalyst support AST at $80\ ^\circ C$ (COR $80\ ^\circ C$), start-up AST at $30\ ^\circ C$ (SU AST), sequence of electrocatalyst/start-up AST (Combined); while local resistance at segment 1 is named SU SEG1.

Accelerated start-up AST and further validation till 1000 cycles.

To develop the AST, the real-world representativeness has been privileged rather than a high acceleration factor. So far, the new start-up AST, presents a transfer function close to 1, till the number of start-up events is limited to few hundreds. The necessity to reduce the time required to perform the AST must be carefully evaluated, because it implies a more complex transfer function. In fact, in general, the higher the acceleration factor, the lower is the AST representativeness of real world, so less accurate will result the transfer function. Here a new procedure is proposed, capable to properly reproduce the start-up/shut-down phenomena in a reasonable timeframe.

By the investigation till here conducted, the platinum dissolution has been recognised as the major cause of materials degradation under mitigated start-up operation. Since, platinum loss is strongly related to the mechanism of platinum oxidation/reduction (PtOx), and accelerated by voltage cycling, the impact of the different zones of voltage profile (as described in Table 9 and depicted in Figure 34(C)) were studied.

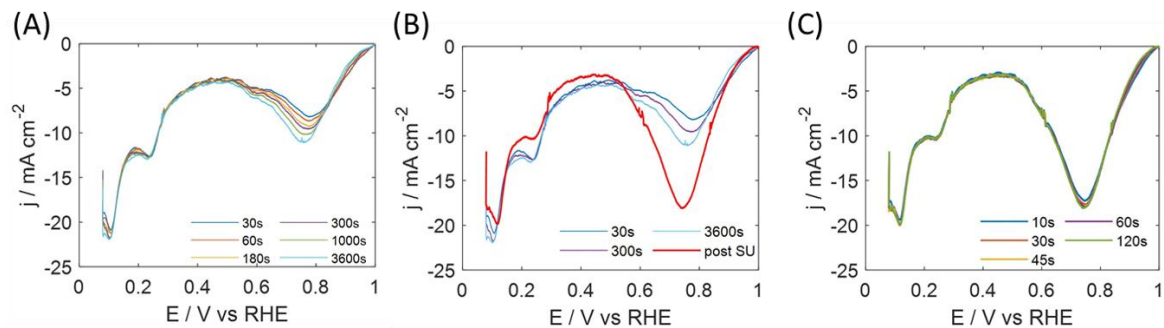


Figure 35 - (A) Effect of holding time on step 2). (B) Effect of start-up 3). (C) Effect of holding time 4).

The results of sensitivity analysis on PtOx formation are reported in Figure 35. keeping the MEA at 1 V for 30 seconds or 1 hour does not significantly change the peak formation. Platinum oxides reach a quasi-steady state after few seconds at high potential, and the subsequent increase in reduction charge follow a logarithmic profile in time. The simulation of regions one and two together was performed introducing the 1.5 V peak (red curve in Figure 35(B)) after a 240 s holding at 1 V. Less than a second at 1.5 V causes a dramatic increase of the reduction charge associated to the oxides respect as seen in the previous operations. In Figure 35(C), the effect of the holding time after start-up is reported. PtOx formation is not significantly affected by the holding time at 1 V, as its increase does not alter the reduction peak previously caused by the high voltage sweep.

Analysis to improve acceleration factor

On the basis of the analysis carried out on the PtOx formation and reduction, a new accelerated protocol is proposed. The times of the basic protocol and the accelerated protocol are presented in Table 10. To evaluate the effect of acceleration and extend the validity of the transfer function from



the accelerated AST with respect to the real aging profile, the analysis of the mitigated start-up/shut-down protocol was extended till 1000 cycles.

Table 10 - Comparison between start-up AST and accelerated start-up AST.

	Refresh at 0.1 V vs RHE	Holding at 1 V vs RHE	Start-up at 1.5 V vs RHE	Holding at 1 V vs RHE	Total duration
Start-up AST	300 s	240 s	0.6 s	120 s	660 s
Accelerated start-up AST	30 s	30 s	0.6 s	10 s	70 s

The results of the mitigated test in segmented-cell are reported in Figure 36. This test was repeated on the JM MEA and the GDL Freudenberg feeding the gas in counter-flow configuration. The ECSA trend, reported in Figure 36(A), confirmed the stress on the cathode electrode in the cathode inlet region. Moreover, the results at 200 cycles are compatible with the first test. After 1000 cycles, the degradation mainly affects segments 1 and 2 with a reduction of the ECSA of more than 80%. The local polarization curves at different aging cycles were compared between cathode inlet (SEG 1) and cathode outlet (SEG 4), and the results are shown in Figure 36(C-D). The performance loss for segment 1, after 1000 cycles, is approximately 230 mV at 1 A/cm² while it is negligible for segment 4. The trend of the oxygen transport resistance at different roughness factor is reported in Figure 36(B). A strong linear correlation is observed confirming what was observed up to 200 cycles. Ex-situ analyses are ongoing to confirm the degradation mechanism up to 1000 cycles.

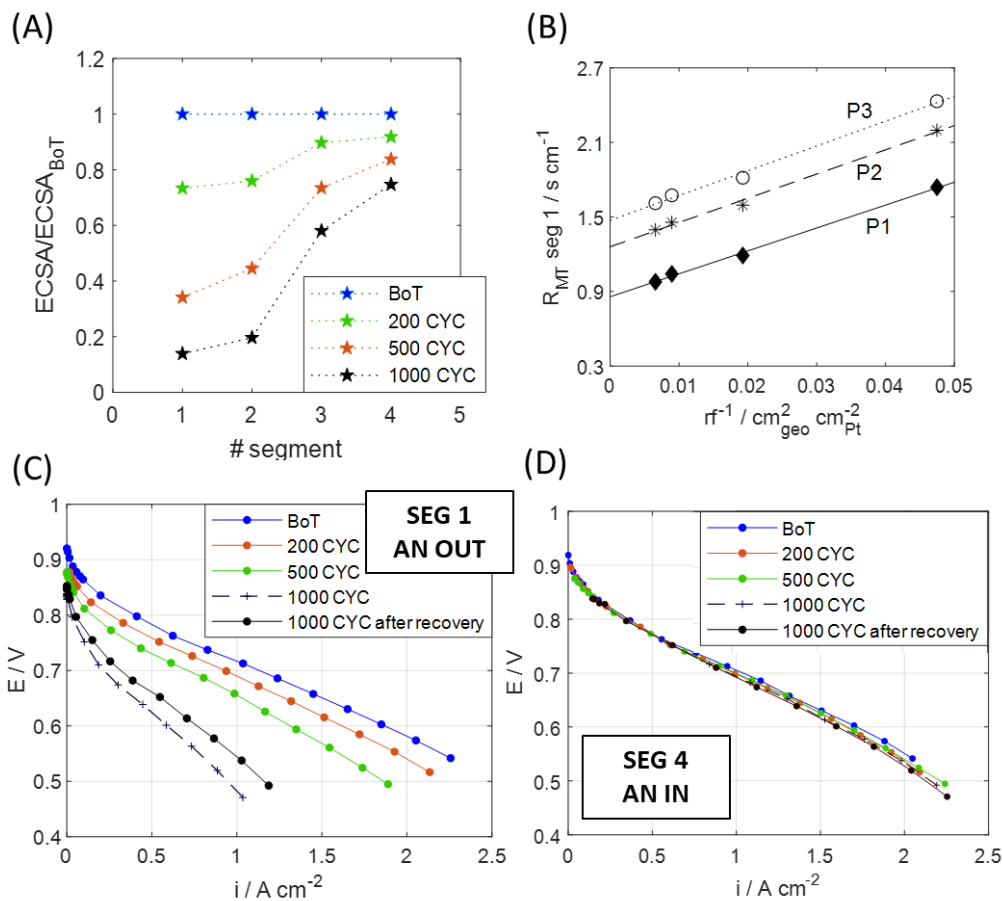


Figure 36 - (A) ECSA evolution in segmented cell, cathode inlet at position at segment 1. (B) Oxygen transport resistance at segment. (C-D) Comparison between H_2 /Air polarization curve performed at segment 1 and segment 4.

Currently, the evaluation of the accelerated protocol, as described in Table 10, is still on-going. Two different maximum potentials are considered: at 1.5 V as in the original start-up AST and at 1.6 V to clarify the stressor effect of maximum potential. In case of fast 1.5 V protocol, for 200 cycles the rate of voltage loss results in $41 \mu V/cycle$, that is comparable to the value of $40 \mu V/cycle$ identified for the original SU-AST with an acceleration factor of 1. ECSA loss results in a 23% decrease, comparable to the 21% of the first protocol. Even the accelerated AST reproduces well what happens in real stacks if, as expected, the number of unmitigated start-up is limited (in the range of 1 every 200 hrs, as specified within the project, up to 1 every 30 hrs). For larger values of unmitigated start-up, ageing mechanisms still need to be clarified through ex-situ analysis.

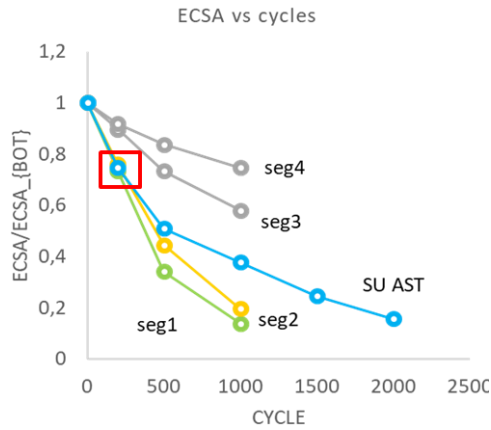


Figure 37 - ECSA evolution in segmented cell compared to ECSA evolution in accelerated SU AST up to 1.5 V.

In order to understand the role of maximum potential during the transient, the same accelerated protocol has been reproduced adopting both 1.5 V and 1.6 V. Tests have been stopped as a minimum ECSA condition was reached (*i.e.* $4.5 \text{ m}^2 \text{ g}^{-1}$), that corresponds to 2000 cycles for 1.6 V protocol and 1500 cycles for 1.5 V protocol. Polarization P results are compared in Figure 38(A). Losses are very similar up to 500 cycles of start-up. Then, the 1.6 V protocol undergoes a larger drop in performance. The voltage losses are depicted in Figure 38(B), for three different current values - low (0.14 A cm^{-2}), medium (1.25 A cm^{-2}) and high current value (2.9 A cm^{-2}). While the 1.5 V protocol shows almost a linear trend for the entire cycles range, it is clear the sudden variation for the 1.6 V protocol in case of high currents. By a simple linearization, the rate of voltage decay is almost 1.4 times larger for the 1.6 V rather than the 1.5 V protocol (see Table 11).

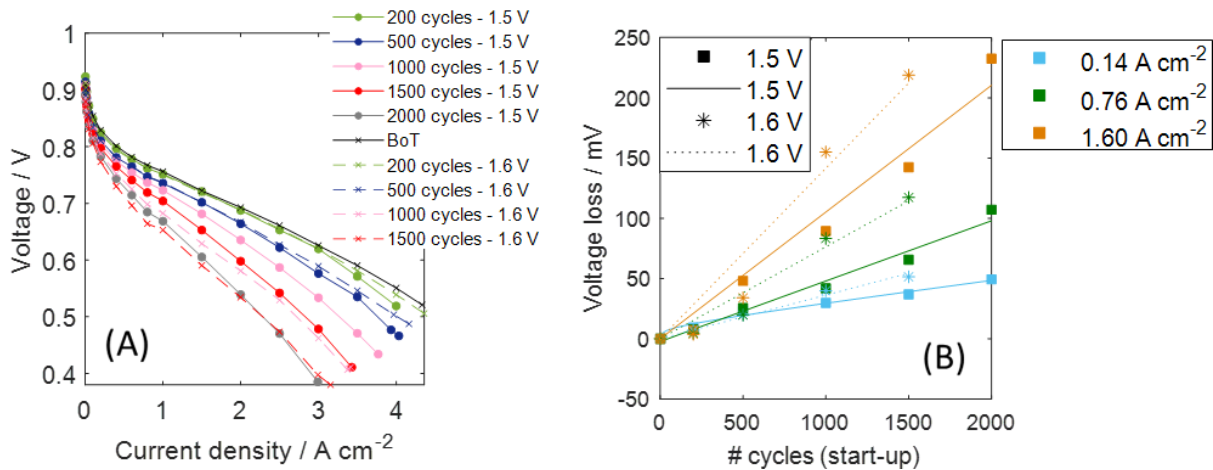


Figure 38 – (A) Polarization P recorded for JMFC aging under accelerated SU-AST protocol, with maximum potential value of 1.5 V and 1.6 V; (B) Voltage loss for three current setpoints for JMFC aging under accelerated SU-AST protocol, with maximum potential value of 1.5 V and 1.6 V.



Table 11 - Comparison between the rate of voltage decay in case of accelerated start-up AST up to 1.5 V and 1.6 V for three different current setpoints.

Rate of voltage decay / $\mu\text{V cycle}^{-1}$		
	1.5 V	1.6 V
0.14 A cm^{-2}	26	36
1.25 A cm^{-2}	49	76
1.90 A cm^{-2}	105	142